A Novel Immunoassay Platform Enabled by Non-fouling Poly(OEGMA) Surfaces

by

Angus Hucknall

Department of Biomedical Engineering
Duke University

Date:_____

Approved:

_____
Ashutosh Chilkoti, Supervisor

_____
Michael Freemark

_____
Gabriel Lopez

_____
Benjamin Yellen

_____
Stephan Zauscher

Dissertation submitted in partial fulfillment of
the requirements for the degree of Doctor
of Philosophy in the Department of
Biomedical Engineering in the Graduate School
of Duke University

2014

ABSTRACT

A Novel Immunoassay Platform Enabled by Non-fouling Poly(OEGMA) Surfaces

by

Angus Hucknall

Department of Biomedical Engineering
Duke University

Date:_____

Approved:

_____
Ashutosh Chilkoti, Supervisor

_____
Michael Freemark

_____
Gabriel Lopez

_____
Benjamin Yellen

_____
Stephan Zauscher

An abstract of a dissertation submitted in partial fulfillment of the requirements for the degree of Doctor of Philosophy in the Department of Biomedical Engineering in the Graduate School of Duke University

2014

Abstract

The primary barriers to multiplexed point of care immunoassays are: (1) cost; (2) response time; and (3) sample handling. Described herein is a self-contained, multiplexed immunoassay platform for point of care detection that leverages a number of enabling technologies to address these barriers. This platform is referred to as the "**D4**" assay, as it is composed of the following four sequential, concerted events (Figure 1): (1) **D**ispense (droplet of blood); (2) **D**issolve (printed reagents on chip); (3) **D**iffuse across surface; (4) **D**etect binding event.

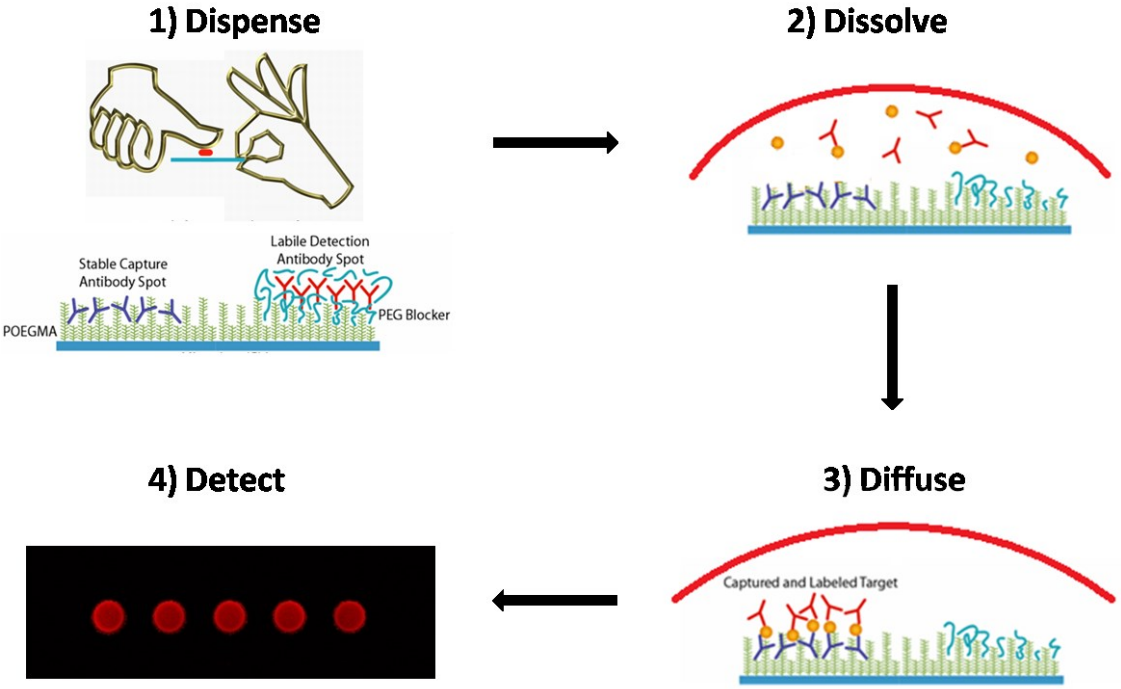

Figure 1: Schematic of the D4 Assay.

The D4 assay process begins when a finger-stick is administered and the resulting droplet of blood is applied to the surface of a detector chip. Hydrophobic ink printed onto the surface of the chip confines the blood droplet to a non-fouling region containing soluble, labile spots of detection antibodies and insoluble, non-labile spots of capture antibodies. As the soluble detection antibodies are dissolved from their printed spots by the droplet of blood, three serial events occur to generate signal (Figure 2): (1) the first half of the detection complex is formed by the binding of analytes present in blood to the stable capture agent spots; (2) diffusion of the blood laterally through the polymer brush, resulting in the dissolution and diffusion of soluble detection antibody spots; (3) solubilized detection antibodies bind to their respective analyte-capture agent spots, completing the detection complex and resulting in signal generation at the position of the non-labile capture antibody spots.

This assay relies upon the ability of labeled detection antibodies, printed into a nonfouling brush as "labile spots", to be carried by blood flow to adjacent rows of stably immobilized capture antibodies by diffusion of the analyte solution (Figure 2). Generation of signal at a given capture spot location provides identification of individual analytes (positives). Quantification of the concentration of the different analytes is carried out identically to a conventional fluorescence immunoassay by pre-calibration of the system using a dilution series of the analyte spiked into whole blood.

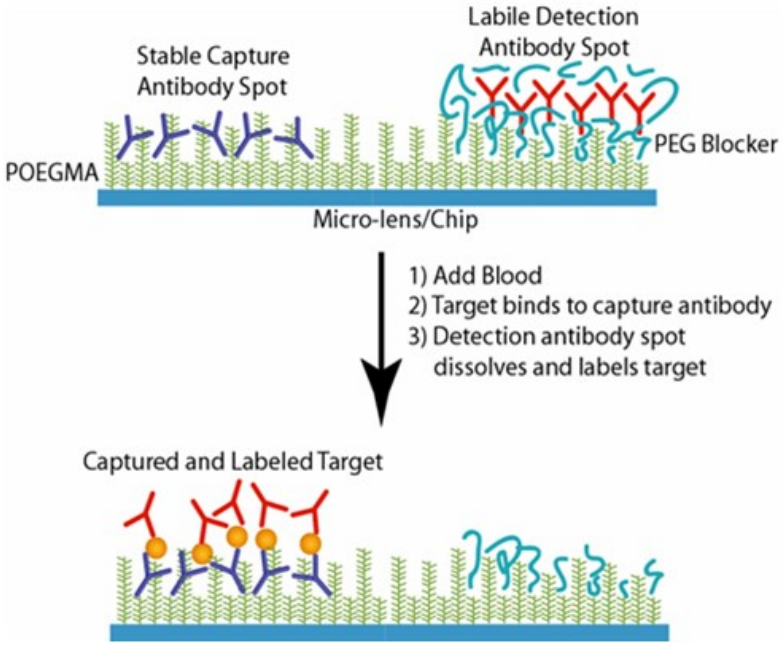

Figure 2: D4 assay format. Two types of spots are printed on the chip: 1) stable spots of capture antibodies, which capture the analyte from blood and form the bottom half of the detection complex, and 2) soluble detection antibody spots which dissolve, label the target, and form the top half of the detection complex

The D4 assay addresses several critical needs in point of care testing: *First*, the cost of testing is reduced through miniaturization, multiplexing and one-step, on-site processing of undiluted whole blood obtained from a finger stick. *Second*, in order to simplify the immunoassay process, the D4 relies on diffusion to bring spatially localized reagents together to create a functional assay and thereby eliminate the need for liquid transfer steps, microfluidic manipulation of sample or reagents, and wash steps. *Third*, this multiplexed platform is capable of screening for a panel of markers in a single drop of blood with no sample preprocessing. *Fourth*, the assay is fast, which alleviates the

difficulties often associated with communicating the outcome of diagnostic tests. A prototype of the D4 assay is shown in Figure 3 below.

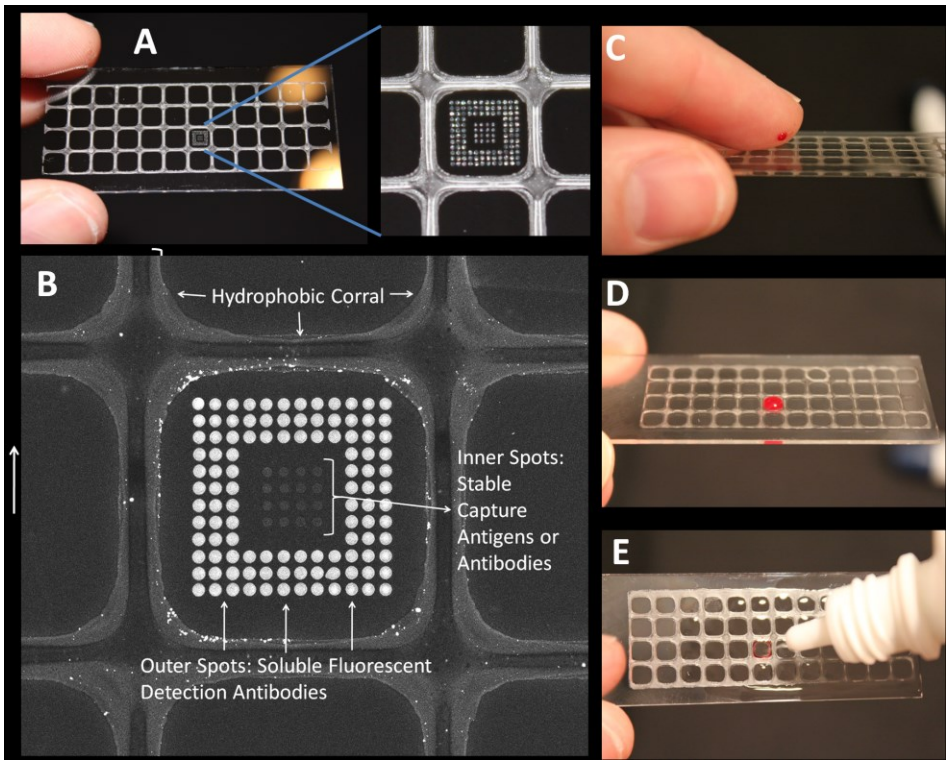

Figure 3: (A) Glass slide with POEGMA brush is stamped with grid of wax, and an antibody array is spotted in the center of a single wax corral. (B) Magnification of inner 4x4 antibody array surrounded by spots containing soluble fluorescent detection antibodies. (C-E) Actual assay—(C) Dispense blood, (D) incubate for 5 min; and (E) displace blood droplet with 1 mL of eyedrops from squeeze bottle. All images were acquired by handheld digital camera except image (B), which was acquired with a fluorescence slide scanner.

Contents

List of Tables

List of Figures

Summary

This document traces the evolution of the D4 point of care test (POCT) platform over the past decade, which occurred in three stages. In the first stage from 2003-2006, Ma and Chilkoti developed a protein and cell resistant surface coating by surface initiated polymerization of a PEG-containing monomer that is widely applicable to different materials such as gold, glass, and plastics; these results are summarized in sections 1.2, 1.3 and 3.1 and references therein. In the second stage, described in sections 1.5 and 3.2, we developed the precursor of the D4 POCT. This was a conventional antibody microarray that allowed multianalyte sandwich immunoassays to be carried out on the POEGMA rush. This precursor platform has the following important attributes that were highly relevant to the subsequent development of the D4 POCT: (i) Capture antibody spots are printed on the POEGMA brush by inkjet printing with no covalent chemistry—this greatly simplifies fabrication of the D4 POCT; (ii) Printed chips can be stored at ambient conditions with no need for hydration or refrigeration for over two months because the POEGMA brush provides sufficient interfacial bound water of hydration to preserve antibody structures at room temperature, which eliminates the "cold chain" required for storage of most antibody functionalized surfaces; (iii) The platform requires only 10-20 μl of blood depending on the number of analytes to be tested, and because the POEGMA brush resists protein adsorption and cell adhesion, it enables sandwich fluoro-immunoassays to be carried out in whole blood. This

precursor platform solved many of the problems of POCTs, but did not solve the problems of reagent incubation and rinse steps or the need for a cheap and portable point of care detector (a conventional fluorescence microarray slide scanner was used for quantification of this precursor platform). In the third and current stage of evolution of this POCT platform, described in sections 4, 5 and 6, we focused on: (1) developing a self-loading and sealing chip design to contain the blood in order to address safety concerns; (2) eliminating all reagent incubation and rinse steps via a passive, 2-D diffusion driven mixing design, and (3) developing a low cost 3-D printed detector that works with a smart phone camera to provide quantitative readout of the assay. Each of these steps in the development of the D4 POCT is described in greater detail in the following sections.

1. Review of Non-fouling POEGMA Surfaces

Protein resistant or "non-fouling" surfaces are of great interest for a variety of biomedical and biotechnology applications. This chapter briefly reviews the development of protein resistant surfaces, followed by a description of a specific methodology to fabricate non-fouling polymer brush surfaces by surface-initiated polymerization. These polymer brushes present short oligo(ethylene glycol) sidechains and are exceptionally resistant to protein adsorption and cell adhesion.

The importance of the protein and cell resistance conferred by these surface tethered brushes is illustrated by their use as substrates for the fabrication of antibody microarrays that exhibit femtomolar limits of detection in complex fluids such as serum and blood with relaxed requirements for intermediate wash steps. This example highlights the important point that the reduction in background noise afforded by protein resistant surfaces can greatly simplify the development of clinical immunoassays with increased sensitivity and utility.

1.1 Introduction

The use of protein resistant or "non-fouling" surfaces is of great interest for a variety of biomedical devices where the prevention of unwanted adsorption of proteins is critical to the performance of the device.[1] Examples of applications in which reducing protein adsorption can be beneficial range from *in vitro* diagnostics where adventitious adsorption can compromise the sensitivity of the diagnostic, to *in vivo*

applications such as biomedical implants where protein adsorption can lead to an undesirable sequence of events that can include thrombus formation or fibrosis and scar tissue formation. Indeed, the importance of protein resistance in medicine and biotechnology spans length scales from the macroscopic to the molecular: modification of the macroscale surfaces of clinical diagnostics with protein resistant polymers can significantly increase their analytical sensitivity, while modification of nanoscale drug delivery vehicles, such as polymer micelles and liposomes, and the molecular surfaces of protein pharmaceutics with this class of polymers can confer long *in vivo* circulation times and thereby improve their efficacy.*[2]* As an example of the practical utility of protein resistance, this chapter will demonstrate the important point that the reduction in background noise afforded by protein resistant surfaces is an often overlooked alternative to signal amplification for the development of heterogeneous –surface based– clinical and proteomic assays with high signal to noise and consequently low limits-of detection (LOD).[3]

To date, the most common approach to reduce protein adsorption on a surface is via a coating of poly(ethylene glycol) (PEG).[4] Although the kinetic and thermodynamic origins of the protein resistance of PEG are still debated,[5-11] studies over the last few decades have shown that surface modification with long-chain PEGs (nominally defined as PEGs with a molecular weight of ≥ 2000 Da) can significantly reduce protein adsorption. Consequently, many methods to immobilize PEG on surfaces

have been developed that include physisorption,[12-15] chemisorption,[16-18] covalent grafting of PEG onto surfaces,[19, 20] and plasma polymerization of oligo(ethylene glycol) (OEG) precursors.[21] With the exception of plasma polymerization, these approaches involve the deposition of PEG onto a surface from solution. Grafted or adsorbed PEG on surfaces decreases the adsorption of proteins, but most of these approaches to surface modification with PEG or PEG-containing copolymers do not reduce the adsorption of proteins below the nominal limit of several ng cm-2, which can be considered a useful operational definition for protein resistance as it is the approximate limit-of-detection (LOD) of most label-free interfacial detection techniques such as surface plasmon resonance (SPR).[22] The limited success of physisorption and covalent grafting (the "grafting to" approach) in reducing protein adsorption has been attributed to the low surface density of PEG chains on the surface (e.g., < 4 μg cm-2),[23] because of the excluded volume effect.[24, 25]

A breakthrough in the development of protein resistant materials came from the work of Prime and Whitesides, who showed that self-assembled monolayers (SAMs) of OEG-terminated alkanethiols (OEG-SH) confer protein resistance to gold, as determined by SPR.[16] Although OEG-SH SAMs on gold exhibited significantly better protein resistance than grafted PEG, they have several limitations. Substrates which can be modified with these SAMs are limited to metals, and because SAMs are a single molecular layer, they have limited robustness, which is further exacerbated by the

existence of defects in the SAM[26-28]and the propensity of the chemisorbed thiolate to oxidize.[29, 30] Nevertheless, OEG-SH SAMs yielded two important insights into the protein-resistance of PEGylated surfaces. First, they clearly demonstrated that long chain PEGs were not essential to limit the adsorption of proteins, as OEG-SH SAMs outperformed most surfaces modified with longer chain PEGs. Second, studies by Grunze and colleagues on the origin of the non-fouling properties of OEG-SH SAMs on gold suggested that their protein resistance is controlled by two primary structural features: the terminal hydrophilicity of the head-group combined with the formation of a dense, but disordered OEG brush with significant penetration of water into the OEG-SH SAMs.[6] Together, these insights suggested that alternative macromolecular architectures (*i.e.*, those other than linear, long chain PEGs) might also confer protein resistance to surfaces.

Recognizing that methods to synthesize non-fouling coatings that combine the advantages of SAMs –high surface density and ease of formation– with those of polymers –thicker, more robust films with versatile architecture and chemistry– are of significant interest for a variety of applications, Chilkoti et al. focused their attention on surface-initiated polymerization (SIP) to investigate the *in situ* synthesis of a high density coating of a PEGylated polymer at a surface.[31] SIP is carried out by the immobilization of a polymerization initiator onto a surface, followed by polymerization of the desired monomer solely from the surface. SIP was chosen because it had been

shown to enable the synthesis of polymer brushes with a high surface density of up to ~8.5 μg cm-2 with good control of surface thickness.[32, 33] Chilkoti et al. hypothesized that coatings of this nature would be a prerequisite for protein resistance, based on the findings of Whitesides, Grunze and others.[6, 16, 34]

Many polymerization mechanisms have been realized in a SIP format, including living cationic and anionic polymerization,[35, 36] ring-opening metathesis polymerization,[37, 38] condensation polymerization,[39, 40] free radical polymerization,[32, 41-43] and atom transfer radical polymerization (ATRP).[44-47] The Chilkoti group chose ATRP largely because it is simple to perform, affords good control of polymerization kinetics, and is compatible with a range of solvents. The commercial availability of oligo(ethylene glycol) methacrylate (OEGMA), a PEG-like, ATRP-compatible monomer, also made ATRP a convenient choice.

1.2 Growth of POEGMA functionalized polymer brushes on surfaces

Using surface initiated atom transfer radical polymerization (SI-ATRP), poly(OEGMA) brushes have been grown on gold and silicon oxide.[31, 48, 49] Figure 4 shows the scheme that was employed to grow poly(OEGMA) from gold and glass. [48] In the example shown here, the attachment of the initiator was achieved by the synthesis of bifunctional molecules that contained an ATRP initiator at one end (a bromoisobutyrate moeity), and a thiol (Figure 4B) or silane (Figure 4C) moiety at the

other end, to allow one-step functionalization of the surface with the initiator via the formation of an alkanethiol SAM on gold or a silane layer on glass.

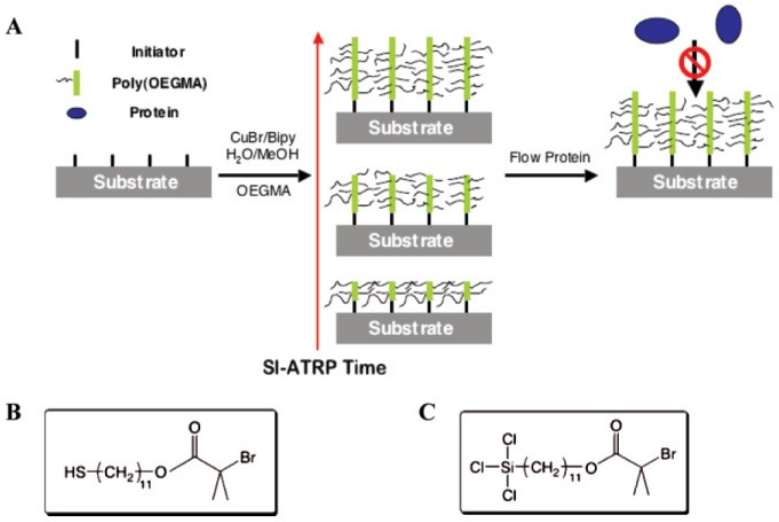

Figure 4: (A) Schematic illustration of SI-ATRP of OEGMA strategy to create a protein-resistant surface. Molecular structure of (B) thiol-terminated initiator, and (C) silane-terminated initiator. [48]

We have recently used an alternative method for the attachment of the ATRP initiator on glass, which does not require independent synthesis of the bromoisobutyrate-terminated silane. The glass surface is initially functionalized with a commercially available, amine-terminated silane, which is easily modified to present the bromoisobutyrate initiator, and is described in the enabaling technologies chapter.[3, 50]

ATRP in general, and that of OEGMA in particular, has several important attributes that are relevant for the modification of surfaces of diverse materials with a protein resistant coating. First, ATRP initiators can be easily immobilized onto surfaces by various methods such as covalent coupling, Langmuir-Blodgett deposition, plasma

grafting and chemical self-assembly.[51, 52] Second, the footprint of the poly(OEGMA) "bottle brush" that is created is significantly larger than that of the initiator, which allows a high density poly(OEGMA) brush coating to be synthesized from a relatively low surface coverage of initiator;[49] this feature is especially important for materials that are likely to yield a low surface coverage of the initiator. Third, ATRP is a "living polymerization" and allows easy control of the polymer graft density and thickness, which are important parameters that can be used to control the protein resistance of these coatings.[44] Fourth, ATRP is compatible with a range of solvents and can be carried out at room temperature, which makes it compatible with a variety of substrate materials. These attractive attributes of ATRP have led to its use for the *in situ* polymerization of diverse monomers from the surface of silicon, silicon oxide, and metals such as Au, Ti, and stainless steel.[48, 53, 54]

1.3 POEGMA surfaces resist protein and cell adhesion

Poly(OEGMA) polymer brushes are exceptionally resistant to protein and cell adhesion; in an initial study, it was observed that the adsorption of fetal bovine serum on a poly(OEGMA) film grown from a single component bromosiobutyrate-terminated alkanethiol SAM (*i.e.*, from a high surface concentration of the initiator) was below the 1 ng cm-2 LOD of SPR (Figure 5A).[49] In order to determine the minimum surface density of initiation sites that would provide protein-resistant polymer brushes, poly(OEGMA) coatings were synthesized by SI-ATRP from binary SAMs of thiols 1 and

2 (Figure 5A)[49] on gold, where the solution –and hence surface– concentration of the initiator was systematically varied across the entire range of possible compositions. SPR measurement of the adsorption of plasma proteins such as fibronectin and fibrinogen from single component solutions, as well as that of proteins from complex protein mixtures such as undiluted fetal bovine serum, revealed a useful design metric for the synthesis of protein-resistant poly(OEGMA) coatings by SI-ATRP: irrespective of the starting concentration of the initiator on the surface of gold, poly(OEGMA) coatings that exhibited an ellipsometric thickness of ≥ 10 nm in their dry state exhibited exceptional resistance to protein adsorption, presumably because these coatings present a high enough surface density of OEG moieties at the solid-water interface to prevent the adsorption of proteins (Figure 5B)[49]. These results were also validated on glass, where poly(OEGMA) layers with a thickness of ≥ 10 nm also resulted in undetectable levels of adsorbed protein, as measured by ellipsometry (LOD of ellipsometry ~1 Å) (Figure 5C)[48]. The protein resistance of poly(OEGMA) brushes has been confirmed by a number of groups, including Katira et al who found that adsorption of kinesin was 20 fold lower on poly(OEGMA) surfaces compared to OEG-SH SAMs on gold.[55]

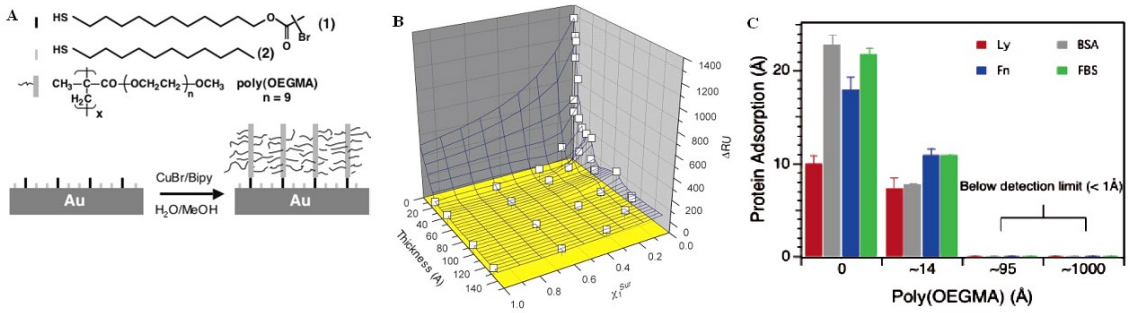

Figure 5: A) Schematic showing the SI-ATRP of OEGMA from a mixed SAM of an initiator-functionalized thiol 1 and a diluent thiol 2 on gold. B) Three dimensional plot of BSA adsorption on poly(OEGMA) surfaces studied by SPR (scattered squares, 36 data points). The thickness of the poly(OEGMA) layer is plotted versus the mole fraction of thiol 1 in the initiator deposition solution, with the corresponding BSA adsorption as measured by SPR plotted on the z axis. C) Protein adsorption onto the poly(OEGMA) brush on silicon oxide and initiator silane modified silicon oxide (control) measured by ellipsometry. The x-axis is the thickness of poly(OEGMA) coatings (or initiator silane as control, labeled as a film with 0 Å thickness), and the y-axis is the thickness of the adsorbed protein. Legend: Ly (lysozyme), Fn (fibronectin), BSA (bovine serum albumin), FBS (fetal bovine serum).[49]

SI-ATRP of OEGMA (and other monomers) is also compatible with various methods of patterning (Figure 6)[31]. An ATRP initiator with a terminal thiol group was patterned on gold by microcontact printing (μCP), followed by SI-ATRP to yield micropatterns of poly(OEGMA) (Figure 6A). Ma et al. also showed that polymer brushes can be patterned at the nanoscale by using dip pen nanolithography (DPN) to pattern the initiator-terminated thiol, followed by SI-ATRP of OEGMA (Figure 6B and C). The protein resistance of poly(OEGMA) brushes also translates to excellent cell resistance, and allows facile patterning of proteins, as the protein-resistant regions of

poly(OEGMA) in the micropatterns prevented the adhesion and outgrowth of cells on these regions, leading to conformal patterns for up to 30 days (Figure 6 D and E).

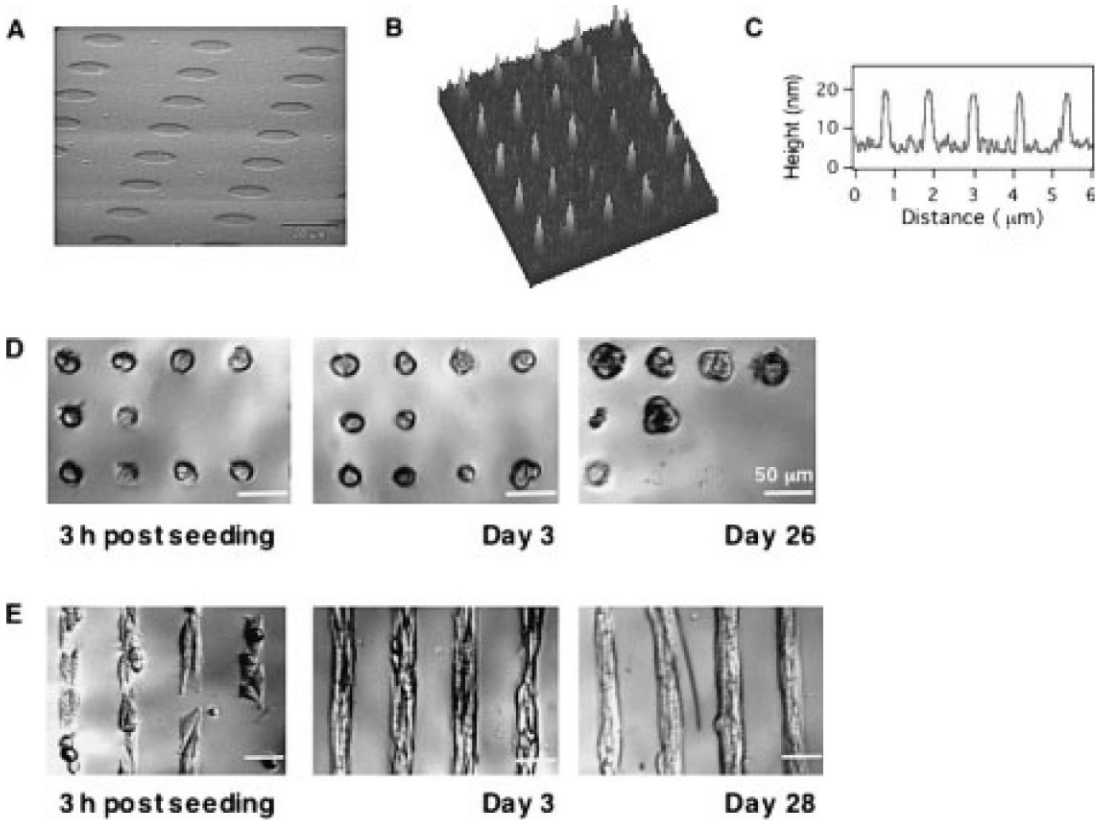

Figure 6: Patterns of poly(OEGMA) brush and attached cells. A) SEM image of a patterned poly(OEGMA) brush on gold that was fabricated by μCP of thiol initiator followed by SI-ATRP of OEGMA. B) Three-dimensional image of a poly(OEGMA) nanoarray over a 5μm x 5μm area grown from the initiator thiol patterned using DPN on gold. C) The line profile of (B) shows that the poly(OEGMA) nanostructures have a diameter of ~90nm and a height of ~14nm. D,E) NIH 3T3 fibroblasts cultured on a pattern of adsorbed fibronectin (20μm circles (D) and 40μm stripes (E)) separated by cell-resistant regions of poly(OEGMA) brushes fabricated by SI-ATRP on gold.[31]

In the interim, it has also become increasingly clear that PEG-containing polymers are not the only materials that confer protein resistance to surfaces. Whitesides and coworkers screened SAMs with different headgroups, and found that certain

zwitterionic headgroups reduced protein adsorption on the SAM to levels that were comparable to the OEG-SH SAMs.[56] Jiang and coworkers have translated these findings to a polymer architecture by growing polymer brushes by SI-ATRP that present zwitterionic side-chains, and have shown that these polymer brushes are exceptionally resistant to protein adsorption.[57]

1.4 Biofunctionalized non-fouling surfaces

Poly(OEGMA) brush surfaces can be easily functionalized because they typically present reactive hydroxyl groups on their surface that can be derivatized with complementary reactive moieties. For example, Tugulu et al. modified poly(2-hydroxyethyl methacrylate) and poly(OEGMA) brushes with RGD tripeptides using p-nitrophenyl chloroformate to create surfaces that promote integrin-mediated cell adhesion.[53] Lee et al. activated the hydroxyl groups of poly(OEGMA) with N,N′-disuccinimidyl carbonate in order to form biotinylated poly(OEGMA) films.[58] Xu *et al.* grew binary brushes of poly(poly(ethylene glycol)methacrylate-co-poly(ethylene glycol)methyl ether methacrylate) and activated the terminal hydroxyl groups on the sidechains directly with 1,1-carbonyldiimidazole for the covalent coupling of human immunoglobulin (IgG).[59] In an alternative approach, Lutz et al combined ATRP with click chemistry using the bromine ends of poly(oligo(ethylene glycol) acrylate) for nucleophilic substitution by azides, followed by reaction with alkynes.[60] While acheiving biofunctionalization of the brush through chemical activation is certainly

attractive, caution must be exercised when modifying the brush in this way as this process may affect the non-fouling properties of poly(OEGMA).

1.5 Protein microarrays on Poly(OEGMA) Brushes

A protein microarray is typically a solid substrate with an array of different proteins that are spatially localized on the surface by printing or spotting each protein with micrometer resolution.[61-66] Protein microarrays are used to detect and/or quantify proteins in solution and have been used for a variety of applications.[67-70] The most common type of protein microarray is the antibody microarray, where antibodies are used as capture molecules to detect and/or quantify the concentrations of analytes in solution.[63, 71]

The development of antibody microarrays for proteomics and clinical diagnostics has been limited by: (1) the availability of high affinity and high specificity antibodies for capture and detection of protein biomarkers; (2) the susceptibility of proteins to denaturation upon adsorption; and (3) the propensity of proteins to avidly adsorb to surfaces, commonly referred to as the "non-specific adsorption" problem.[72, 73] In contrast to attempts at improving the performance of protein microarrays by increasing the surface concentration ("loading density") of the capture antibody, as well as sophisticated attempts at signal amplification (both of which simply increase the absolute signal but do not necessarily appreciably increase the signal-to-noise ratio), an often overlooked critical limiting factor that controls the LOD in protein microarrays

(and in fact all surface-based diagnostics) is the threshold of noise in the assay. Excluding receptor specificity for its target as a source of noise (an important problem which biointerface design cannot solve and which requires the development of better antibody selection strategies and antibody engineering approaches such as affinity maturation[74]), we hypothesized that the "biomolecular" noise in heterogeneous immunoassays that stems from the adventitious adsorption of proteins (such as extraneous proteins that are present in the analyte solution) is a primary factor that controls the LOD.

To test this hypothesis, identical antibody arrays were spotted on both non-fouling POEGMA surfaces as well as traditional nitrocellulose surfaces, which exhibit exceptional capture antibody immobilization but suffer from high levels of background noise due to non-specific adsorption. Although the absolute signal from the spotted arrays on poly(OEGMA) was lower than that obtained from arrays spotted on nitrocellulose, the background signal obtained from the poly(OEGMA) (which approached the autofluorescence levels of the glass substrate) was significantly lower than that from nitrocellulose, and the LODs in serum for arrays spotted on poly(OEGMA) brushes were 100-fold lower than the same protein microarrays spotted on nitrocellulose. This clearly demonstrated that despite the lower absolute signal from the antibody arrays spotted on poly(OEGMA) versus nitrocelluose, the significantly lower background fluorescence on the poly(OEGMA) brush more than compensated for

the lower signal. This work is described in detail in the enabling technologies chapter and is only highlighted here as a practical example of the utility of non-fouling surfaces—see section 3.2.2 for experimental details and data.

1.6 Conclusions

Recent work on poly(OEGMA) brushes shows that they have significant utility in lowering the adsorption of proteins from serum/blood to undetectable levels. These studies highlight the important role that contemporary materials and surface science can play in the development of biointerfaces for clinical diagnostics. Specifically, the femtomolar LODs in serum and blood and the wide dynamic range of antibody arrays spotted on poly(OEGMA) brushes prove the hypothesis that lowering nonspecific binding during the interrogation of protein microarrays can lead to significantly lower LODs. The results also suggest that these microarrays may be useful for applications in proteomics and clinical diagnostics that require the quantification of low abundance protein biomarkers directly from complex mixtures such as whole blood.

2. Need for Improved POC Immunoassay Platforms

The following is a description of several barriers inherent in the current immunoassay process, as well as solutions that we believe can reduce these barriers. These same issues often become even more apparent as health workers screen for biomarkers in low resource settings, and the impact of our enabling technologies in this specific arena is described in this section.

2.1 Cost

The most accurate immunoassay-based blood tests for a single marker are enzyme linked immunosorbent assays (ELISA) that cost approximately $16 and six hours of technician time per marker tested.[75] Recent improvements that enable multiplexing are now capable of testing for an array of four markers at a cost of $14 and 4.5 hours of technician time.[75] However, these tests require the use of approximately $110,000 - $160,000 of specialized laboratory equipment.[75] Also, each test requires the use of approximately 200μL of serum or plasma, which must be separated from a sample of whole blood taken from a patient by a venous blood draw. This blood draw is generally taken at the point-of-care and must then be transported to a centralized laboratory for the actual test.

The system described in this work significantly reduces cost by streamlining the key aspects of sample collection, processing and testing as follows: (1) elimination of all preprocessing by directly testing undiluted whole blood, obtained from a finger stick; (2)

test miniaturization to decrease the amount of reagents – the antibodies that are spotted as capture and detection agents; and (3) one-step, on-site processing. In addition, the test is multiplexed and capable of targeting a panel of markers, without significantly increasing cost over that of a single marker test.

It is important to note that this will be achieved without the use of sample preprocessing or the use of microfluidics to separate cells from the analyte solution because of the unique protein and cell-resistant POEGMA polymer brush that allows fluoroimmunoassays to be carried out with femtomolar limits-of-detection from whole blood,[76] which is described in the chapter on Enabling Technologies.

In addition, the novel application of engineered functional surfaces[76-78] allows for the miniaturization of the diagnostic system to significantly reduce the amount of capture agent needed, effectively eliminating one of the most significant costs in standard immunoassay tests, such as plate-based ELISA assays. Further, by employing recently developed techniques of inkjet bioprinting,[79] disposable, multiplexed sensor chips can be manufactured at a cost on the order of several cents per chip.

Relevance of cost reduction to low resource settings: Reducing the cost of the assay offers obvious advantages: test more people for less money. But the cost reduction achieved by reducing the required dependence on a highly developed health care infrastructure is also important—for example, traveling clinics in developing nations have limited time and personnel, and a multiplexed test with single-step, on-site

processing significantly increases patient throughput. In addition, creating a miniaturized, multiplexed assay eliminates vast amounts of materials and significantly reduces the burden of transportation, storage and disposal. In particular, the protein-stabilizing property of our sensor chip surface enables transportation and storage of the chips in ambient conditions, avoiding the need for costly climate-controlled storage and transport.

2.2 Assay Simplicity and Time-to-readout.

More than 50% of patients do not return if a second visit is required to receive test results. In fact, it has been shown that up to 50% of patients will leave before receiving test results if wait time is 100 minutes, and approximately 20% of patients will leave if wait time is 50 minutes.[80] The platform described here has the potential to reduce this problem by providing results within 15 minutes. This helps ensure that both the test and the result are provided during a single visit, which will also remove the need for patients to provide contact information for result notification (providing this information can lead to patient privacy concerns, another reason for test avoidance).

Tests requiring whole blood samples drawn by venipuncture require significant effort, time and the availability of highly skilled workers. In addition to the actual drawing of the blood sample, many diagnostics require that the blood be separated into serum or plasma. This requires additional equipment and expertise, increases assay cost and time-to-readout, and limits the ability to provide point-of-care diagnosis.

Additionally, the process of venipuncture itself can lead to medical complications for the patient, and the strong aversion that many individuals feel toward venipuncture is a significant barrier to testing. All of these concerns can be reduced by creating a test that analyzes just a few microliters of blood, which can be easily obtained via a finger-stick.

By creating a test with the ability to detect multiple targets in only a few microliters of blood, increased access for the testing of neonates becomes possible, where drawing larger quantities of blood is problematic and often requires a blood transfusion at the time of the blood draw due to the quantity of blood required. This has the potential to make a significant impact on the screening of newborns.

Finally, by relying on the same basic principle employed in LFAs—liquid transport via capillary action—this design will eliminate the need for washing or liquid transfer steps. This is a very important point, as there will be no need for expensive or complex microfluidics, which thereby reduces chip cost and eliminates a major cause of failure so common to most contemporary "lab-on-a-chip" designs when they are field-tested with clinical samples.

Relevance of assay simplicity to low resource settings: Higher throughput of biomarker testing will be achieved by reducing required materials (in this case, the elimination of needles and blood collection vials, as well as the concern of their proper disposal) and decreasing personnel burden (eliminating venipuncture and sample pre-

processing). In addition, the only disposable item created in this design, other than the finger stick lancet, is a small piece of glass or plastic, which serves as the assay's blood contacting surface. Thousands of these could be disinfected with a single liter of bleach solution—disposal of these surfaces alongside normal trash would then be possible.

Additionally, testing in low resource settings often occurs in isolated regions. While bringing testing to these areas increases access, it is often the case that any type of follow up is non-existent or occurs only after long periods of time. In addition, face-to-face communication is often the only option, as other methods such as mail, telephone, or e-mail are unavailable or unreliable. For these reasons, rapid results are essential. As mentioned above, options such as lateral flow strip-based tests are available for these situations, but their sensitivity is limited, as is the potential for highly multiplexed tests in this format.

2.3 Sensitivity.

It is our goal to combine the sensitivity found in standard laboratory tests, such as plate-based ELISA assays, with the advantages of inexpensive, hand-held and rapid result lateral flow strip assays. We believe the key to achieving this is our utilization of novel materials in the design of this system. Through the use of an inexpensive surface coating capable of eliminating the non-specific adsorption of biomolecules and cells, this assay should be capable of improving sensitivity through the elimination of adventitious

adsorption of proteins, one of the single largest sources of background noise in bioassays.

Relevance of improved sensitivity to low resource settings: Typically, the most sensitive assays require the support of a technologically sophisticated and capital-intensive healthcare infrastructure, where patient samples are collected at the point-of-care and transported to a lab that maintains the equipment and personnel required to perform the actual test. Low resource settings simply do not have access to such facilities, which precludes these areas from utilizing the most sensitive diagnostics. This system offers on-site analysis, which would allow this highly sensitive diagnostic to be utilized in settings where the health care infrastructure is less developed.

3. Enabling Technologies

The D4 assay retains the most attractive features of the lateral flow assay format, namely the elimination of microfluidics and fast results, but makes significant improvements in sensitivity and usability through a suite of **three enabling technologies**: (1) Synthesis of POEGMA brushes on glass and plastics which eliminate nonspecific binding of proteins and cells; (2) The use of ink jet printing for the non-covalent immobilization of capture antibodies on POEGMA brushes, enabling antibody arrays that have a long shelf-life and provide limits of detection as low as 15 fM in whole blood; and (3) Soluble microspots capable of dissolving into a blood sample and providing the secondary reagents necessary for "sandwich" detection.

3.1 Enabling Technology I: Non-fouling POEGMA brushes

3.1.1 POEGMA brushes can be grown on glass, silicon oxide and plastics

POEGMA brushes can be synthesized by surface initiated atom transfer radical polymerization (SI-ATRP) on glass and silicon wafers (with a thermally grown oxide layer) as shown in Figure 7. First, aminopropyltriethoxysilane (APTES) is used to form an amine-terminated self-assembled monolayer (SAM) on the surface (step 1), followed by attachment of the ATRP initiator –bromoisobutyryl bromide– to the amine groups presented by the APTES SAM (step 2), and subsequent ATRP from a solution that contains CuBr, bipyridine and the monomer –OEGMA– under argon (step 3).This

procedure allowed convenient synthesis of ~100 nm thick films that were found to be useful for printing Abs and other proteins used in immunoassays.

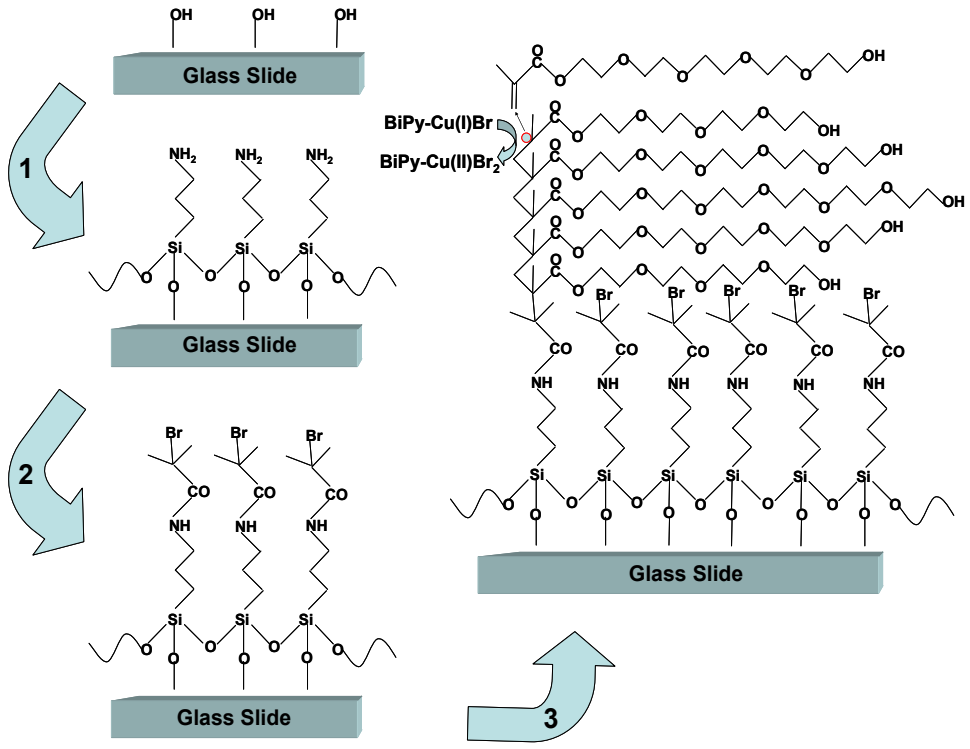

Figure 7: Synthesis of POEGMA brushes on glass via SI-ATRP. Cleaned slides were functionalized with APTES in step 1, and modified to present an ATRP initiator in step 2. Slides were then immersed in a polymerization solution in step 3 to synthesize surface tethered brushes of POEGMA.

For POEGMA brushes grown on glass or silicon, the ATRP initiator can be conveniently immobilized by a silane SAM. However, plastics, which may be a preferred class of substrate materials for the D4 assay, do not support SAM formation. To overcome this limitation, we investigated three substrate-independent methods for deposition of an initiator layer: (1) plasma polymerization of 2-chloroethyl methacrylate (2-CEMA) on glass; (2) dip-coating a range of industrially relevant, planar polymer

substrates (PS, PMMA, PET and PE) in a solution of poly(vinylbenzyl chloride) (PVBC); and (3) spin coating of PVBC on silicon.[77] These layers were then used to initiate SI-ATRP of OEGMA. We chose these methods because: (1) they are capable of functionalizing a broad range of materials, and (2) they do not rely upon custom-fabricated initiators deposited as SAMs.

X-ray photoelectron spectroscopy was used to assess the functionalization of substrates with initiator. The survey scans, summarized in Table 1, provide information of overall surface chemical composition. We found that in all cases, the overall chemical composition matched the expected composition reasonably well. High-resolution C1s spectra (Figure 8) provide insight into the chemical bonding environment of carbon. In Table 1, we compare the observed contributions of each chemical state of carbon to the expected contributions based on the stochiometric ratios present in each chemical structure. In the case of plasma polymerized 2-CEMA, the observed contributions of oxygen and chlorine are less than expected. This is a result of the higher susceptibility of C-Cl and C-O bonds to degradation during plasma exposure.[81] The high-resolution C1s peak of the poly(OEGMA) brushes can be fit with five unique carbon moieties: CHx(285.0 and 285.7 eV), C–O–R (286.6 eV and 287.3 eV), and COOR (289.1 eV).[82]

Table 1: Atomic % From Survey and High Resolution C1s Scans in Figure 8

		C1s					Survey		
		1	2	3	4	5	C	O	Cl
2-CEMA	Observed	46.6	23.3	11.4	10.4	8.1	79.9	14.4	5.6
	Expected	33.3	16.6	16.6	16.6	16.6	66.6	22.2	11.1
2-CEMA-POEGMA	Observed	17.5	8.7	56.1	8.7	8.7	70.3	29.6	-
	Expected	16.6	8.3	58.3	8.3	8.3	66.6	33.3	-
PVBC	Observed	64.2	21.4	14.3	-	-	91.5	.5	7.9
	Expected	66.6	22.2	11.1	-	-	90	-	10
PVBC-POEGMA	Observed	17.2	8.6	56.9	8.6	8.6	70.5	29.0	.5
	Expected	16.6	8.3	58.3	8.3	8.3	66.6	33.3	-

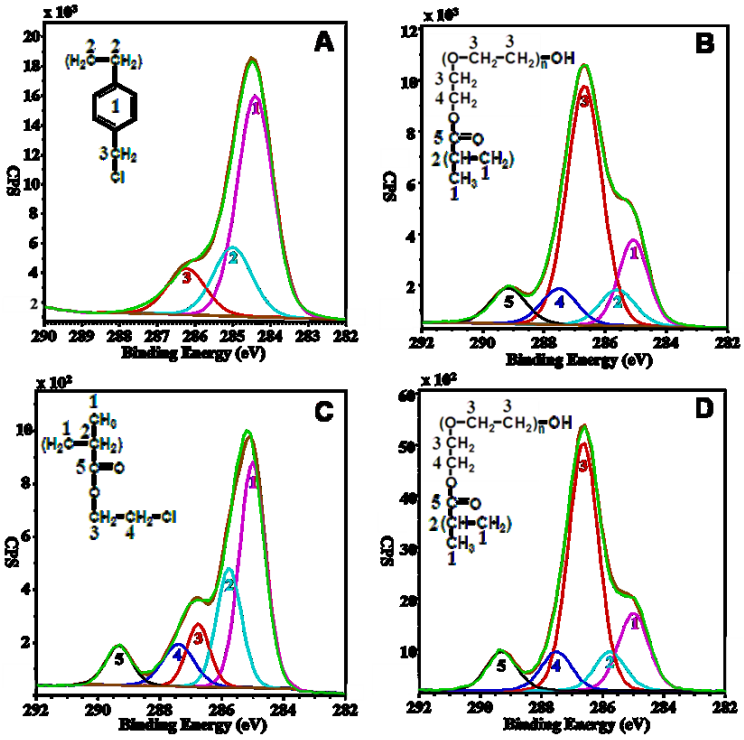

Figure 8: High resolution spectra of the C1s peak and chemical structure (inset) of substrates before (A, C) and after (B, D) OEGMA polymerization on initiator functionalized substrates. Fitted peaks are numbered to correspond with labeled carbons within each chemical structure. Polystyrene dipcoated with PVBC (A) before and (B) after SI-ATRP of OEGMA. Plasma-polymerized 2-CEMA (C) before and (D) after SI-ATRP of OEGMA.

From the deconvoluted C1s spectra of the poly(OEGMA) brush seen in Figure 8 B and D, the sum of components 3 and 4 arising from the pendant oligo(ethylene glycol) sidechains accounts for 64.8% and 65.5% of the total signal, respectively, which is within experimental error. The ratios of the carbon moieties, obtained by deconvolution of the high-resolution C1s spectra of POEGMA brushes synthesized by the three different methods, revealed no significant differences and were close to those obtained previously for POEGMA.[49, 83] These results suggest that our initiator deposition methods are robust and lead to chemically well defined POEGMA brush structures on the variety of substrates tested.

A number of complementary approaches can be used to grow POEGMA brushes on the diverse substrates used for clinical diagnostics: attachment of a bromo group to a silane on glass or a simple dip-coat of the substrate into a solution of a halogen-containing polymer both provide the necessary halogen moieties needed to initiate SI-ATRP of POEGMA brush structures on glass and a variety of industrial polymers. These results strongly indicate the feasibility of coating the top surface of a variety of substrates with the POEGMA brush prior to inkjet printing of capture agents for development of the D4 assay.

3.1.2 POEGMA brushes resist protein and cell adsorption

3.1.2.1 Glass

The protein resistance of the POEGMA brushes grown on silicon wafers was tested by adsorption of fibronectin (Fn), bovine serum albumin (BSA), lysozyme (Ly) (all proteins at 1 mg mL^{-1} in PBS, pH = 7.4), and undiluted fetal bovine serum (FBS). The thicknesses of the protein layers as a function of the POEGMA film thickness was measured by ellipsometry, and are shown in Figure 9.[83] The thickness of the adsorbed protein on the control surface varied depending upon the protein, ranging from ~10 Å (Ly) to ~25 Å for the other proteins and serum. In contrast, a thin POEGMA brush (~14 Å thickness) showed significantly less protein adsorption of all proteins and of serum. Increasing the thickness of the POEGMA brush to ~95 Å or greater eliminated the adsorption of all proteins, and most notably that of serum proteins, to below the 1 Å detection limit of ellipsometry. These results are consistent with our previously published results on gold that a POEGMA brush with ≥10 nm ellipsometric thickness is dense enough to completely resist protein adsorption from serum.[84]

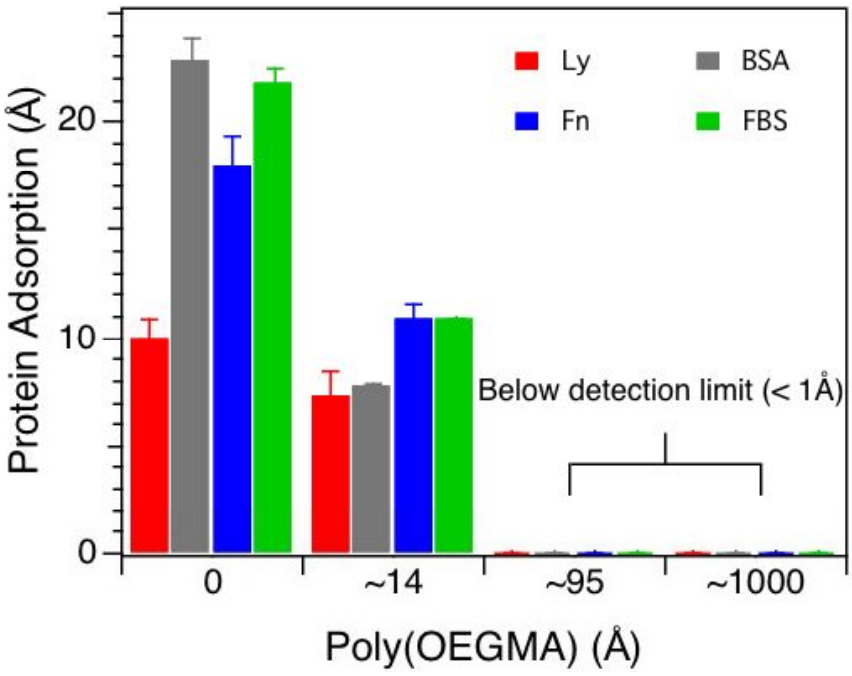

Figure 9: Protein adsorption on POEGMA brushes of different thicknesses on silicon oxide and initiator-silane modified silicon oxide (control: 0) measured by ellipsometry. Legend: Ly (lysozyme), Fn (fibronectin), BSA (bovine serum albumin), FBS (fetal bovine serum).

3.1.2.2 Plastics

The resistance to non-specific protein adsorption of the POEGMA brush layers grown on plasma-deposited initiator layers was evaluated by first incubating the 2-CEMA and 2-CEMA-POEGMA surfaces in undiluted fetal bovine serum for 12 hours, and then subjecting the substrates to XPS analysis. The XPS data in Table 2 show that there is considerable protein adsorption on the 2-CEMA surface (N = 3.2 atomic %) but no detectable protein adsorption on the POEGMA modified substrates. Furthermore, the resistance to non-specific protein adsorption of the POEGMA brush layers grown on plasma-deposited initiator layers was evaluated by first incubating the 2-CEMA and 2-

CEMA-POEGMA surfaces for 12 hours in a solution of human umbilical vein endothelial cells in serum containing media, with subsequent fluorescence imaging of the surface. Figure 10 shows that the POEGMA brushes resisted cell attachment, as no fluorescence could be observed. These results further support the conclusion that these surfaces are protein resistant, as anchorage dependent cells are extraordinarily sensitive to trace levels of adsorption of extracellular matrix proteins such as fibronectin, which can provide anchorage sites for cells via the formation of focal contacts at levels corresponding to RGD surface concentrations as low as 10fmol/cm^2.[85, 86]

These data show that protein-resistant POEGMA brushes completely prevent non-specific adsorption of serum proteins when their thickness is ≥ 10 nm, a feature that is incorporated in the fabrication of the D4 assay by the use of ~100 nm thick brushes.

Table 2: Atomic % from XPS Spectra taken before and after FBS incubation

		Observed Atomic %			
		N	C	O	Cl
2-CEMA	Before	0	79.95	14.4	5.66
	After	3.20	75.07	16.11	5.62
2-CEMA-POEGMA	Before	0	70.32	29.68	0
	After	0	70.33	29.67	0

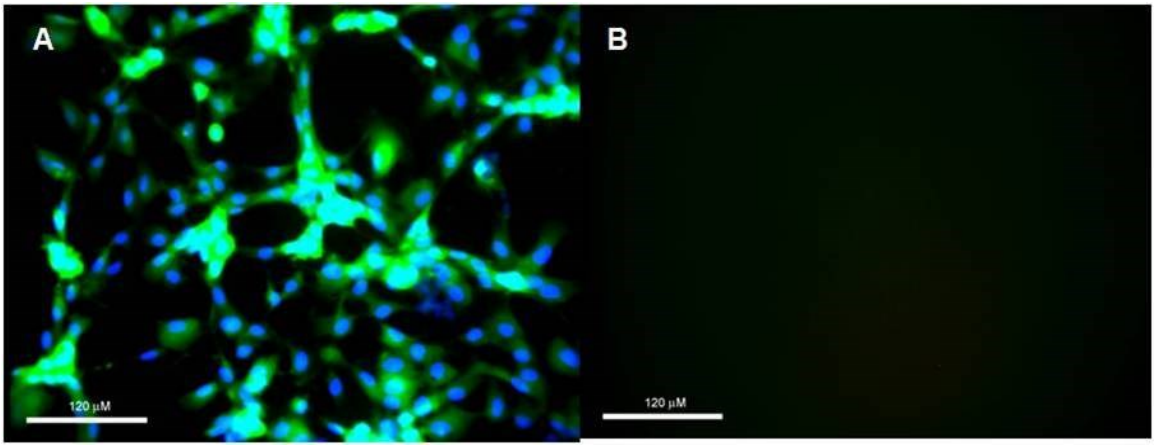

Figure 10: Fluorescence images (20X) of 2-CEMA (A) and 2-CEMA-POEGMA (B) after exposure to HUVECs for 24 hours and subsequent cell staining. The POEGMA coating eliminated cell adhesion. Scale bars represent 120 microns.

3.2 Enabling Technology II: Stable Microspots on POEGMA brushes.

We have discovered a remarkably simple method to print antibodies on a nonfouling polymer that involves adsorption of the antibody into the polymer brush by macroscopic drying of the printed array. The interfacial architecture of the POEGMA traps sufficient water within the brush to enable retention of the antibody's folded

structure, allowing these printed spots to retain their activity even after storage at the lab-bench for many months. This is an important feature that is relevant to the D4 assay, as it means that such printed diagnostics will not need to be stored in buffer at 4 ^{o}C, thereby making this technology very useful as: (1) printed chips can be transported at room temperature, (2) the chips are amenable to use in low resource settings because of relaxed constraints on transportation, storage and handling requirements, and (3) the chips can be used in POC situations where refrigeration may not be easily available.

Capture antibodies were printed as ~150 μm diameter spots on a 100 nm thick POEGMA brush at room temperature and humidity using a PerkinElmer Piezorray™ noncontact printer (Figure 11 and Figure 12A) and were allowed to non-covalently absorb into the 100 nm thick polymer brush. After printing, the spots were dried by placing the printed slides under vacuum to facilitate the absorption of the capture antibody into the polymer brush; *note that this step is necessary as proteins will not adsorb on the polymer brush from solution*. We also observed that the POEGMA coated glass slides could be stored in a closed container and left on the bench-top for up to two months, with no observed degradation in performance of antibody arrays that were subsequently printed on the polymer brushes.

3.2.1 Physically printed antibody arrays are stable upon aqueous exposure.

A solution of 1 mg/mL Cy-5 labeled goat anti-mouse IgG (Jackson Laboratories) was printed on POEGMA coated substrates to produce the arrays shown in Figure 11A.

The arrays were dehydrated for 24 h to promote immobilization of the antibody and then subjected to high power sonication for 10 minutes in a 1% (v/v) Tween-20 solution. This printing and drying process provides stable immobilization of antibody, as the arrayed spots were still visible after high power sonication in a 1% Tween-20 solution (Figure 11B). An advantage of this approach over chemical activation of the POEGMA brushes and subsequent covalent attachment is the extreme simplicity of the process, as no slide activation/deactivation steps are required.[78] Direct physical printing provides highly stable antibody arrays and provides a simple method for fabrication of antibody arrays with minimal processing steps.

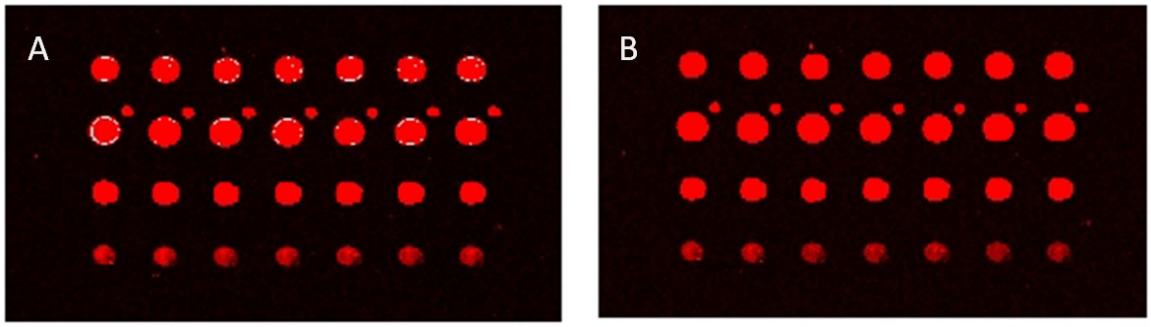

Figure 11: Fluorescently labeled antibody arrays are stable to sonication. (A) As printed array, (B) After 10 min sonication in 1% Tween-20 solution.

3.2.2 Antibody arrays on POEGMA brushes are highly sensitive.

An antibody array specific for IL-1β, IL-6, IL-8, TNF-α and osteoprotegerin (OPG) was directly printed onto a 100 nm thick POEGMA brush grown by SI-ATRP on glass and nitrocellulose.[76] A fluorescence image of microarray spots for an IL-6 assay spotted on POEGMA on glass shows the increase in fluorescence intensity with

increasing analyte concentration (Figure 12A). Remarkably, spots could be visually discriminated from background even at an IL-6 concentration of 5 fM. Figure 12A also shows that the POEGMA matrix retained its ability to resist non-specific protein adsorption throughout array fabrication and the subsequent sandwich immuno-fluorescence assay, as the fluorescence intensity in the background areas surrounding spots measured prior to the assay showed no increase in intensity upon completion of the procedure (the only background fluorescence detected on the POEGMA substrates was due to the autofluorescence of the glass slide). This decrease in the background signal on POEGMA translated to femtomolar limits of detection (LODs) in serum for all five analytes that were tested, and a dynamic range that spans six orders of magnitude of analyte concentration.

The OPG dose response curves in buffer and serum for OPG-specific antibodies spotted on POEGMA (Figure 12B) illustrate another important consequence of the use of a protein resistant substrate, as they show that the LODs are virtually identical in buffer and serum. These results are in contrast to most other fluorescence immunoassays, where the LOD is typically orders of magnitude greater in complex physiological solutions containing high concentrations of extraneous proteins compared to the LOD of the assay in buffer.[73, 87]

Although the absolute signal from the spotted arrays on POEGMA was lower than that obtained from arrays spotted on nitrocellulose (data not shown), the

background signal obtained from the POEGMA (which approached the autofluorescence levels of the glass substrate) was significantly lower than that from nitrocellulose. The fluorescence response of an IL-6 specific antibody array spotted on nitrocellulose and POEGMA as a function of IL-6 concentration in serum are shown in Figure 12C. *The LODs in serum for arrays spotted on POEGMA brushes were 100-fold lower than the same protein microarrays spotted on nitrocellulose*, which clearly demonstrated that despite the lower absolute signal from the antibody arrays spotted on POEGMA versus nitrocellulose, the significantly lower background fluorescence on the POEGMA brush more than compensated for the lower signal from the spots. We also found that antibodies to IL-6 spotted on a POEGMA brush on glass could detect IL-6 directly from undiluted, whole blood with a LOD of ~15 fM (Figure 12D). Clearly, these results demonstrate that the reduction of non-specific protein adsorption is a powerful method for decreasing the LOD by dropping the threshold of noise in the dose-response curve of these assays to concentrations in the sub-picomolar regime.

Because these microarrays were physically spotted on POEGMA and did not involve any covalent coupling of the capture antibody to the substrate, they also have the potential to greatly simplify protein microarray assays by eliminating the need for chemical activation and deactivation of the surface. The ability of these microarrays to resist the adsorption of proteins and cells from solution also provides the ancillary advantages of simplifying and reducing the time needed to perform the assay by

eliminating blocking steps, reducing the rinsing steps during interrogation of the array, and enabling the detection of analytes directly from whole blood. These features eliminate many of the time-consuming and tedious sample processing steps found in most microarray based assays, which will decrease the labor, cost and time required to carry out these assays in a clinical setting, thereby facilitating the use of microarray-based assays as point-of-care diagnostics.

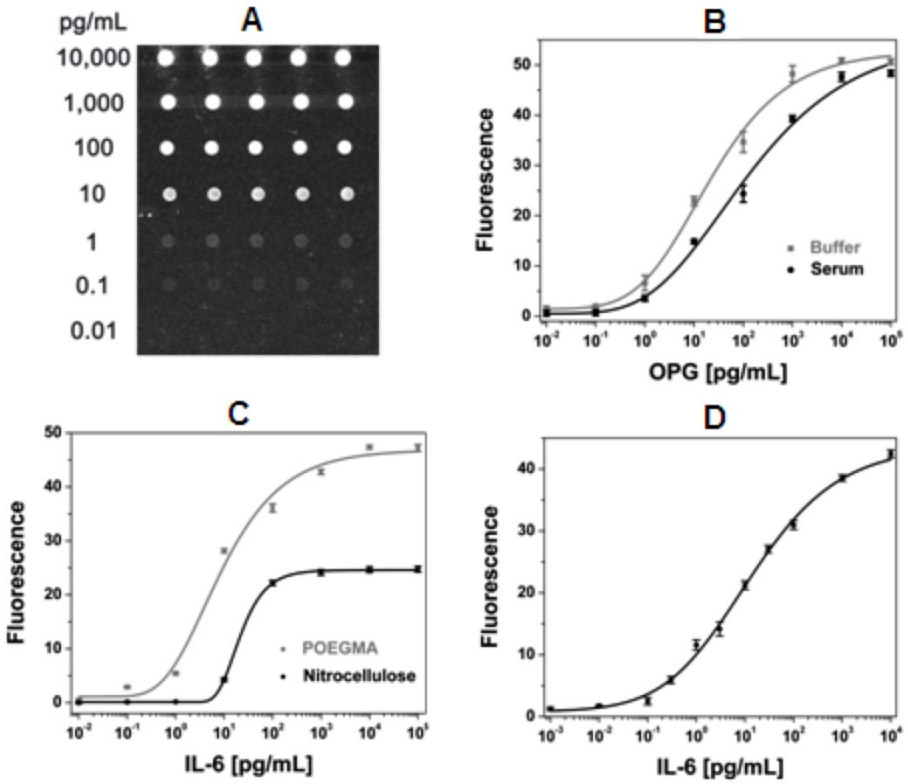

Figure 12: (A) Image of a typical IL-6 microarray interrogated from serum. (B) Dose response curves of OPG in buffer and serum on poly(OEGMA). (C) Dose response curves of IL-6 in serum on poly(OEGMA) and nitrocellulose. (D) Dose response curve for an IL-6 microarray exposed to whole blood. In B-D, the ordinate shows the average background subtracted fluorescence intensity in spots and the abcissa shows the analyte concentration in solution. Error bars represent one standard deviation.

3.3 Enabling Technology III. Soluble microspots on POEGMA brushes

On-chip secondary reagents are necessary for the development of a self-contained immunoassay platform. Novel printing and surface modification methods capable of providing labile microspots will allow secondary detection reagents such as fluorescently labeled anti-human detection antibodies to be printed alongside capture antibody spots. Upon contact with a droplet of blood, these secondary reagent spots dissolve into solution and label target present in the blood sample. Concurrently, the labeled targets contained within the sample bind to the immobilized, non-labile capture spots (Figure 13).

By printing a blocking-agent into the POEGMA brush and varying the solution components of the printed secondary reagents, it is possible to create labile spots which dissolve into solution. Soluble PEG serves two important roles in this process. First, a PEG solution is printed prior to printing the secondary reagents, where it is adsorbed into the POEGMA brush and blocks adsorption of the detection agents into the brush layer. Additionally, soluble PEG is added to the spotted solutions of secondary reagents, where the untethered PEG stabilizes activity of the detection agents during storage, and facilitates dissolution upon contact with the analyte solution.

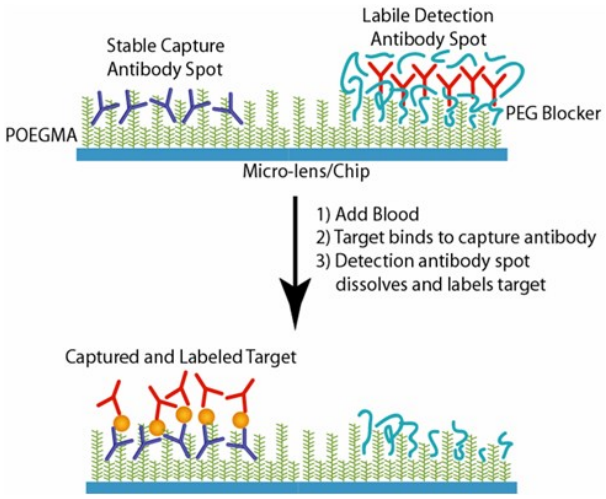

Figure 13: Two types of spots are printed on the chip: 1) stable spots of antigen ("capture agents"), which capture the analyte from blood and form the bottom half of the detection complex, and 2) soluble detection antibody spots which label the target and form the top half of the detection complex.

As an initial proof-of-principle experiment to illustrate the feasibility of this approach, an array of biotinylated antibody spots was printed onto a POEGMA surface. In addition, a solution of streptavidin-Cy5 and soluble PEG was spotted on top of pre-printed spots of soluble PEG. After one week, 50uL of PBS was added to these arrays in order to test the ability of the streptavidin-Cy5 spots to dissolve into solution and bind to the biotinylated-Ab capture spots. As seen in Figure 14, a sufficient amount of active Cy5-streptavidin dissolved into solution and was captured by the biotinylated-Ab spots to create a detectable signal.

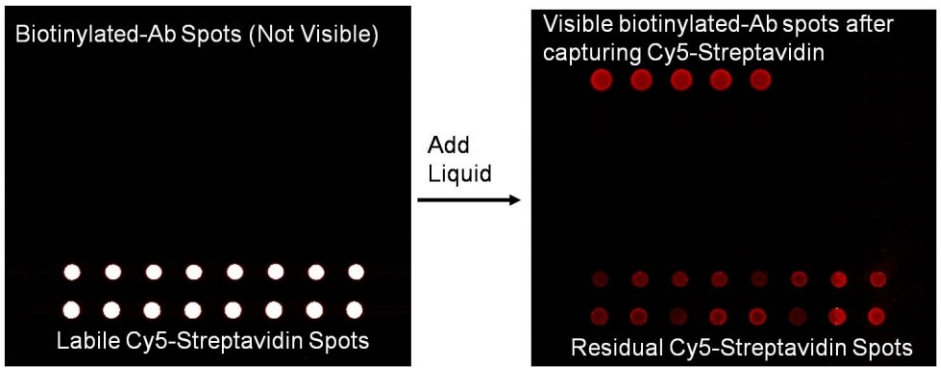

Figure 14: Proof-of-principle experiment demonstrating feasibility of printing capture and detection agents simultaneously. Labile Cy5-streptavidin spots dissolved into solution and subsequently bound to biotinylated-Ab spots after addition of buffer.

Two approaches were evaluated for their effect on dissolution of the printed detection antibody: (1) Soluble PEG added to the print solution of the detection antibody, and (2) Soluble PEG pre-printed directly into the POEGMA brush prior to printing of the detection antibody. In investigating both of these approaches, the primary variable used to optimize dissolution of the printed detection antibody spots upon aqueous exposure was the molecular weight of the soluble PEG.

In order to determine the effectiveness of adding PEG to the print solution, an array of stable anti-BNP capture spots were printed alongside experimental soluble spots, as well as a negative control row of anti-PSA capture antibodies, as shown in Figure 15 below. 50uL of buffer containing 1 ng/mL BNP was then added to the array, which allowed the labeled detection antibody spots to dissolve into solution and label any BNP captured by the stable anti-BNP spots. Upon scanning, two parameters were used to evaluate the effectiveness of the soluble PEG: signal generated at the stable anti-

BNP spots after capture of BNP and labeled Cy-5 anti-BNP, and the intensity of the soluble Cy-5 anti-BNP detection antibody spots remaining due to lack of dissolution and/or residual antibody trapped within the brush. By comparing the level of residual intensity to the level of captured intensity, an estimation of the ability of the PEG additives to both promote detection reagent dissolution and preserve detection reagent activity can be made. For example, low levels of residual intensity coupled with low levels of captured intensity would suggest that while the soluble detection agent microspots dissolved well, the solubilized Cy-5 anti-BNP Ab did not bind to the captured BNP, presumably due to loss of biological activity caused during the drying process.

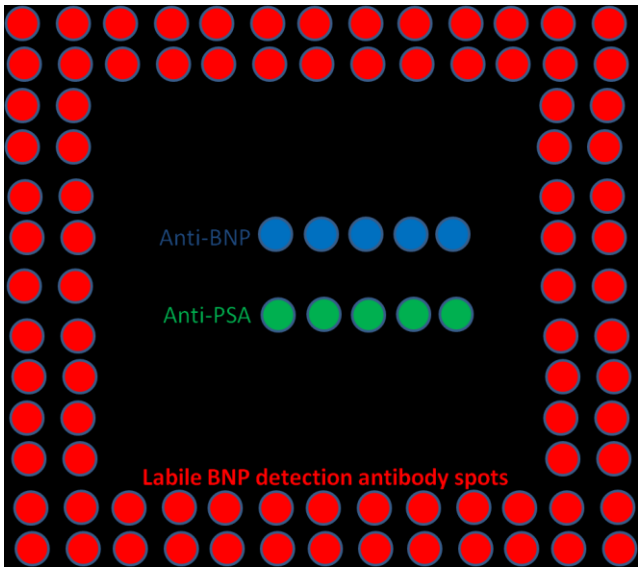

Figure 15: Array format for soluble microspot tests

3.3.1 Approach 1: Soluble PEG Added to Detection Agent Print Solution.

Three molecular weights of PEG were evaluated: 960, 11600, and 66800 Da. Each of these was added to the print solution of a Cy-5 labeled anti-BNP antibody at 1mg/mL. Buffer containing 1 ng/mL BNP was then added to the array, which allowed the Cy-5 anti-BNP spots to dissolve into solution and label the BNP. Upon scanning, the major parameter used to evaluate the effectiveness of the soluble spots was the signal generated at the position of the stable capture spots, which was taken as a direct measure of the availability of the dissolved detection antibody. The highest levels of active, dissolved detection antibody were observed when PEG of 11,600 and 66,800 MW were added to the print solution(Figure 16)—no significant difference in captured fluorescence was observed between these two molecular weights. Of these two molecular weights, we have chosen to use the 11,600 MW PEG because it consistently produces fewer errors during printing, presumably due to our printer's preference for lower viscosity fluids.

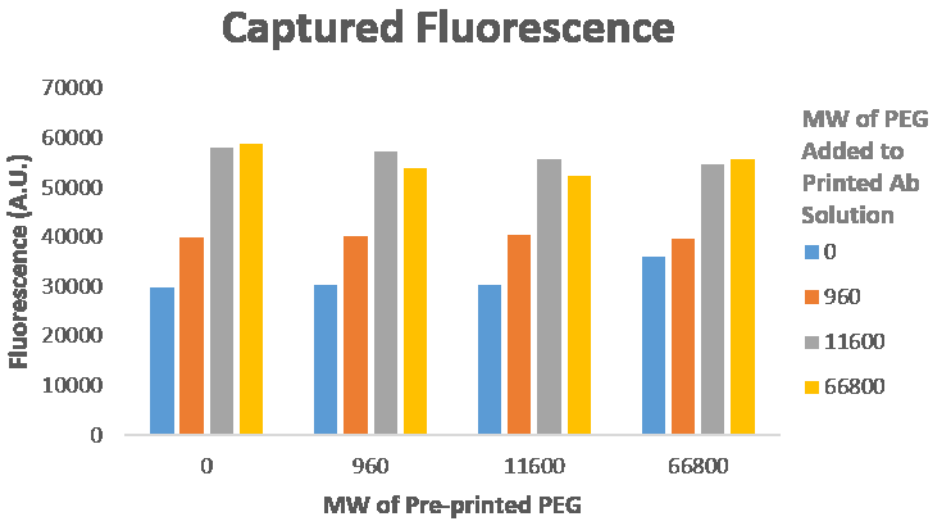

Figure 16: Fluorescence of capture antibody spots due to specific binding of solubilized detection antibodies as a function of PEG MW

3.3.2 Approach 2: Soluble PEG Directly Pre-printed into the POEGMA Brush.

In a second approach to promote dissolution of microspots of detection reagent, soluble PEG was printed on the POEGMA brush prior to printing the detection antibodies on top of these spots of pre-printed PEG. It was expected that this pre-printed PEG would adsorb into the brush and thereby block the adsorption of detection agents, enabling a higher degree of dissolution of the detection agent microspots. 1% w/v solutions of PEG with molecular weights of 960, 11600, and 66800 Da were printed into the brush prior to printing microspots of detection antibody. The effect of pre-printing PEG into the POEGMA brush was evaluated by comparing the residual intensity of detection agent spots (Figure 17) after BNP spiked buffer was added to the

array. Higher molecular weight PEG pre-printed into the brush produced lower residual spot intensities, suggesting that the longer PEG chains were more efficient at blocking adsorption of the detection antibody. However, the amount of additional detection antibody made available by blocking adsorption into the brush with pre-printed PEG did not have a significant effect upon the signal intensity observed at the position of the capture spots (Figure 16). Presumably, the amount of additional detection antibody that dissolved into solution due to the pre-blocking of the surface was such a small percentage of the total dissolved detection antibody that no significant difference in binding to the capture spots was observed. As such, the pre-printing of PEG into the POEGMA brush was not carried forward as part of the optimized printing protocols resulting from this work. However, this technique may prove useful in future assay design. As the device continues to be miniaturized, it is probable that stable capture spots and soluble detection spots will be located in closer proximity. This will create greater potential for residual fluorescence from the detection spots to complicate quantification of the signal of capture spots. Therefore, pre-printing of PEG in order to reduce residual intensity may prove useful in order to reduce the likelihood of the residual fluorescence signal from the detection spots interfering with the quantified signal of the capture spots.

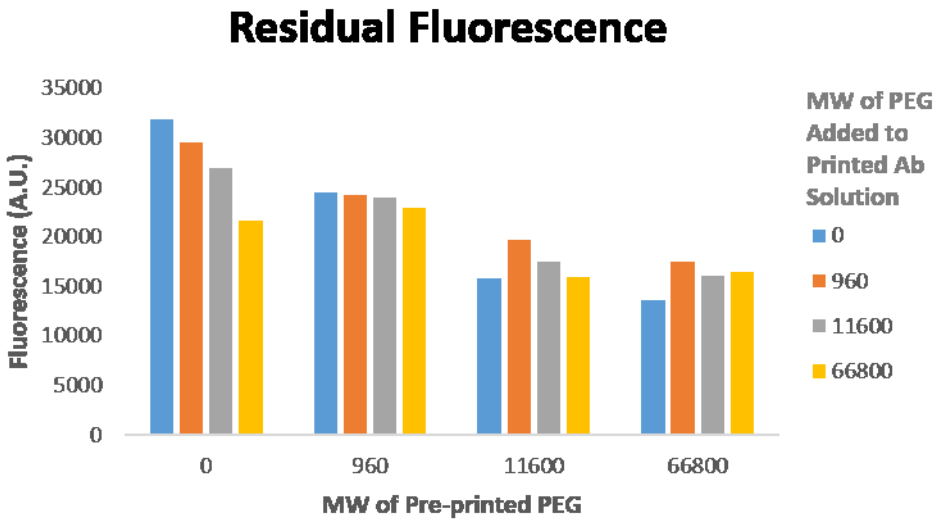

Figure 17: Residual fluorescence of detection antibody spots as a function of PEG MW.

In conclusion, the development and use of "labile" microspots allows the D4 assay to contain on-chip secondary reagents, which enable an all-in-one, self-contained assay. This format simplifies the sandwich assay process by eliminating the numerous wash and liquid transfer steps typically required for secondary reagent addition and removal.

3.4 Materials and Methods

3.4.1 Surface functionalization of substrates with 3-aminopropyltriethoxysilane

Unless otherwise stated, all steps described herein are performed under ambient conditions. 75 x 25 mm pre-cleaned glass slides (Schott Nexterion Slide B) were individually placed in a Teflon slide rack. In addition, a silicon wafer with 20 nm thermal oxide (Si/SiO2) (University Wafer) diced to similar dimensions was added to the

slide rack to enable serial monitoring of organic film layer thickness via reflective ellipsometry. 25 g of 3-aminopropyltriethoxysilane (APTES) (Gelest) was added to a glass bowl filled with 400 mL 200 proof ethanol (Koptec) while stirring, and subsequently the rack with slides was slowly immersed and left stirring in this solution overnight. The slides were then rinsed in pure ethanol and three times in 18 MΩ deionized water (DI), centrifuged at 150 rcf for 6 minutes to remove water, and placed in an oven pre-heated to 100 degrees Celsius for 1 hour. Reflective mode ellipsometry (J.A. Woollam Co.) was then performed on the silicon wafer to measure thickness of APTES layer, which typically corresponded to about 5 angstroms.

3.4.2 Attachment of polymerization initiator to APTES layer

Slides were immersed in dichloromethane, to which 5 mL triethylamine (Sigma-Aldrich) and 5 mL bromoisobutyrylbromide (Sigma-Aldrich) were added while stirring. After 30 minutes the slides were then rinsed with fresh dichloromethane (BDH Chemicals), ethanol, and then 3 times with DI, then centrifuged at 150 rcf for 6 mins. Reflective ellipsometry was performed on the Si/SiO2 chip to quantitate the increase in organic film layer thickness after immobilization of initiator to the surface, which typically corresponded to an additional 3 angstroms (8 angstroms total).

3.4.3 Growth of polymer brushes on initiator-functionalized slides

50g of inhibitor-free POEGMA (Sigma-Aldrich) was added to 400 mL DI. 10 mL each of 0.02 M aqueous solution of 2,2'-Dipyridyl (Sigma-Aldrich), 0.01 M aqueous

solution of copper (II) bromide (Sigma-Aldrich), and 0.35 M ascorbic acid (Fluka) were prepared. All the above solutions were then degassed for 1 hour and together with the surface-functionalized slides were taken into a glovebox purged with argon. The dipyridyl and copper (II) bromide solutions were added to the POEGMA/DI solution while stirring, at which point the reaction solution turned light blue; next, upon adding the 0.35M ascorbic acid solution, the reaction solution turned reddish brown. The entire brown reaction solution was then poured into a glass bowl containing the functionalized slides. The slides were left in the reaction solution with gentle stirbar agitation for 5 hours. Upon removal from the polymerization solution, slides were rinsed 4 times with DI, and then centrifuged dry at 150 rcf for 6 mins. Reflective ellipsometry was performed on the Si/SiO2 chip to assess the thickness of the POEGMA polymer brushes on the slides, which typically corresponded to 50nm.

3.4.4 Synthesis of POEGMA brushes on plastic

3.4.4.1 Spincoating

Following Dressick et al.,[88] Si wafers were first vapor treated for 10 min with a 10% (v/v) solution of hexamethyldisilazane in acetone in a closed container to promote the adhesion of the spin-coated poly(vinylbenzyl chloride) (PVBC) initiator layers. A solution of 1% (w/v) PVBC in toluene was prepared and filtered through a 0.2 μm pore Teflon filter immediately prior to spin coating at 3000 rpm for 30 s. The coated wafers

were baked in a vented oven at 90 °C for 30 min to remove excess toluene from the PVBC film.

3.4.4.2 Dipcoating

Poly(styrene) (PS), poly(methyl methacrylate) (PMMA), poly(ethylene terephtalate) (PET) and poly(ethylene) (PE) samples used in the preparation of dip-coated PVBC initiator layers were first cleaned with isopropyl alcohol to remove organic surface contaminants. The substrates were then dipped into a solution of 10% (w/v) PVBC in toluene for one second and allowed to dry. Dip-coating was repeated twice and the samples were then placed in a vacuum oven at 50 °C for 30 min to remove excess toluene from the PVBC film.

3.4.4.3 Plasma Polymerization of Initiator

Glass cover slips (15 mm, Ted Pella), used for the deposition of plasma polymerized initiator layers were first etched in argon for 5 minutes at 40 W. The coverslips were then coated with 2-CEMA (Pfaltz and Bauer, Inc, heated to 33 °C) for 1 minute at 80W in order to form an adhesion layer, after which the power was lowered to 10W for 5 minutes and finally to 5W for 5 minutes. A pressure of 250 mT was maintained throughout the entire process.

3.4.4.4 OEGMA polymerization on plastic substrates

To grow POEGMA brushes on the dip-coated, spin-coated, and plasma-polymerized surfaces, substrates were immersed in a ATRP polymerization solution of

CuBr (143 mg, 1.0 mmol), bipyridine (312 mg, 2.0 mmol), deionized water (degassed, 3 mL), methanol (12 mL), and OEGMA (8 g, 16.7 mmol).[31, 48, 49] After a specified time under nitrogen purge, the samples were removed from solution to stop the polymerization, then rinsed with methanol, and dried under a stream of N_2 gas.

4. The D4 Assay

4.1 Proof-of-concept of the D4 assay in blood.

The first proof-of-concept of the D4 assay in blood was the detection of human IgG and IgM. These analytes were chosen for their relatively high concentration in blood and because healthy donor blood can be used for this purpose. Figure 18 shows the fabrication of the assay.

First, a ~30 nm thick POEGMA brush was grown on a glass slide by SI-ATRP. The coated glass slide was stamped with a grid pattern of wax using a slide imprinter to confine blood samples to the active area of the chip (Figure 18A). Creating a prototype in this format on a standard 1"x3" slide with a slide imprinter that creates a grid of wax corrals was chosen for its convenience and availability, but in practice, each test would simply correspond to an array (immobile + labile spots) within a single hydrophobic corral on an appropriately sized glass or plastic chip. An antibody array was next inkjet printed in the center of a single wax corral; each spot is ~150 μm in diameter. The inner 4x4 array contains spots of capture antibodies (Ab_c) that comprise the "stable" capture spots— rows 1 and 4 are an anti-murine Ab_c (positive control); row 2: anti-human IgG Ab_c; row 3: anti-human IgM Ab_c. Next, the detection cocktail was printed as 3 outer rows of "labile" spots (Figure 18B). These spots contain a mixture of murine Cy-5-anti-human-IgG and/or murine Cy-5-anti-human-IgM (detection antibodies with a different epitope

against human IgG and IgM than the capture antibodies), and were printed as a solution containing 1% PEG (11,600 Mw).

The images in Figure 18A were acquired with a digital camera while Figure 18B was acquired on a fluorescence scanner. The inner 4x4 antibody array has no intrinsic fluorescence and is only visible in Figure 18B because of light scattering from the printed Ab solutions. The outer spots are visible because they contain Cy5-labeled detection antibody at a high enough concentration that they saturate the detector and hence appear white.

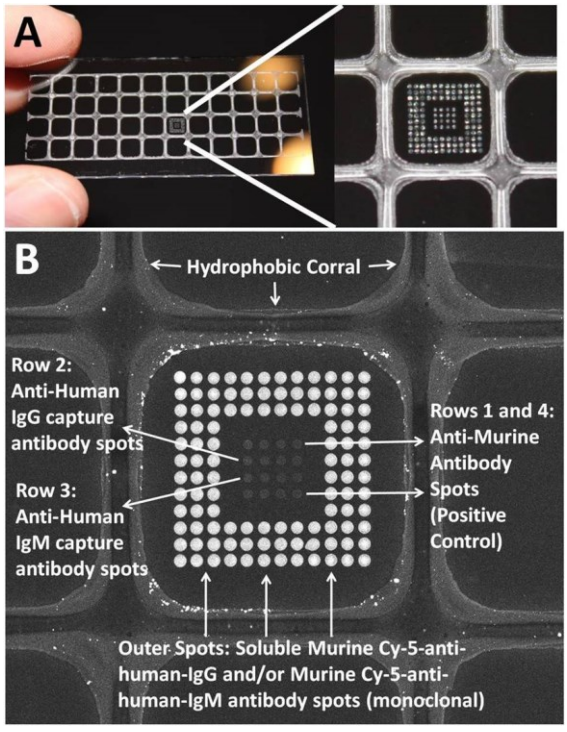

Figure 18: Glass slide with POEGMA brush is stamped with grid of wax. (A) Antibody array is spotted in the center of a single wax corral. (B) Magnification of inner 4x4 antibody array surrounded by spots containing soluble fluorescent detection reagents. Images in (A) were acquired by a digital camera, while (B) was acquired by a fluorescence scanner.

Figure 19 shows photographs of an actual assay. A drop of blood from a finger stick (~10 μL) (Figure 19A) is applied to the surface of a D4 assay chip within the hydrophobic corral, and incubated for 5 min (Figure 19B). The surface is quickly rinsed with ~1 ml from a squeeze bottle, which displaces the loosely bound blood cells and proteins. Interestingly, the blood binds to the hydrophobic corrals, as seen from the red color around the margins (Figure 19C), but is completely removed from POEGMA coated surfaces.

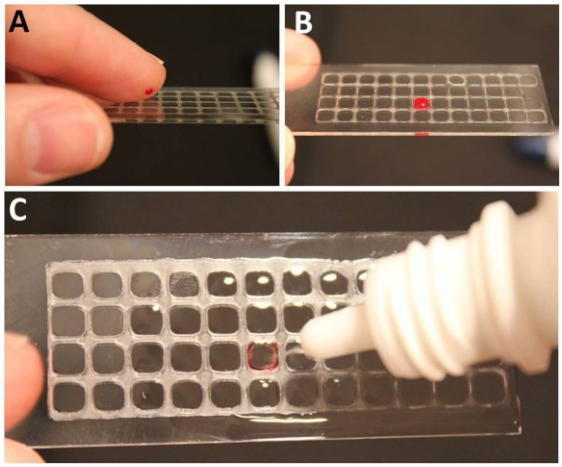

Figure 19: Actual assay. (A) Dispense blood, (B) incubate for 5 min; and (C) wash with 1 mL from Visine™ bottle.

Figure 20 shows the output of the D4 assay. In Figure 20B, detection antibodies for human IgG and IgM were co-printed as labile detection spots, so that a complete sandwich is created upon incubation in blood, leading to fluorescent spots appearing in both rows 2 and 3. The red margins in Figure 20B-F are simply due to scattering from the blood (and excess detection antibody) bound to the hydrophobic corral after displacement from the POEGMA brush by the rinse step. In whole blood, the

concentration of IgG is roughly 5 mg/mL (33 μM) and that of IgM is 1.5 mg/mL (1.6 μM),[89] suggesting that protein analytes can easily be detected from undiluted blood at this level even in this initial experiment. Figure 20E and Figure 20F show negative control experiments in which the chip was incubated with either chicken blood (E) or PBS (F) so that only the positive control rows 1 and 4 generate signal, while rows 2 and 3 show no fluorescence. Figure 20C and Figure 20D are two additional controls; in Figure 20C, only the Cy5-anti-IgG detection antibody was printed in the labile spots, so that signal is generated at row 2 but not at row 3, while in Figure 20D, only the Cy5-anti-IgM detection antibody was printed in the labile spots, so that row 3 generates signal, while row 2 does not. Note that the Cy5-detection antibodies were printed at high concentrations in the outer circumference of labile spots, and are only partially dissolved upon contact with blood, so that their residual fluorescence still saturates the detector.

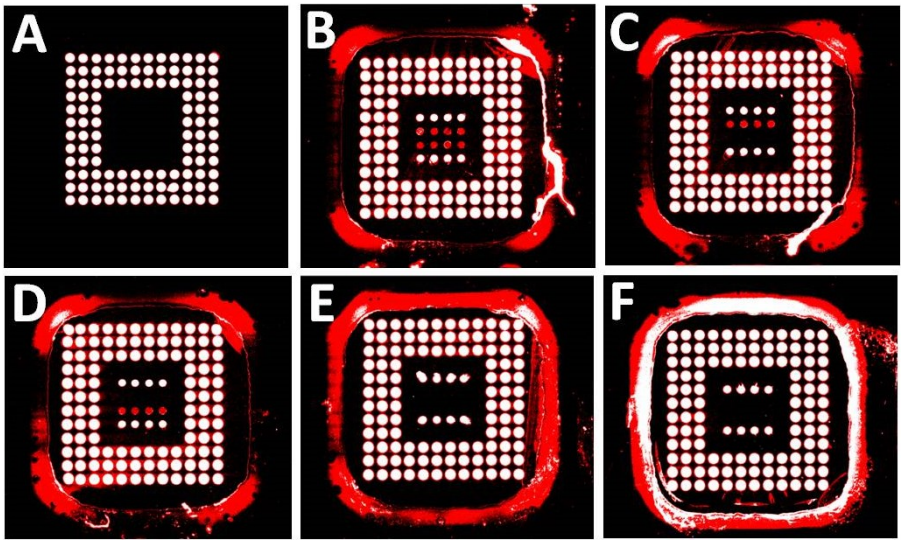

Figure 20: Results of D4 assay for human IgG and IgM in whole blood. (A) Printed assay prior to liquid exposure. (B)-(D) After 10 μL of human blood for 5 min followed by rinse. (B) Cy5-anti-IgG and Cy5-anti-IgM spotted in the outer rows of 'labile' detection spots. (C) Only Cy5-anti-IgG in labile detection spots. (D) Only Cy5-anti-IgM in labile detection spots. (E) After 10uL whole chicken blood. (F) After 10uL PBS.

4.2 D4 Assay for Markers of Cardiovascular Disease

Because IgG and IgM have micromolar concentration in blood, we next used a multiplexed assay for two markers of cardiovascular disease to quantify the sensitivity of the D4 assay.

Cardiovascular disease (CVD) is a global epidemic of unparalleled proportion, with atherosclerotic coronary heart disease (CHD) representing the largest and most rapidly increasing component, followed by congestive heart failure and venous thromboembolism.[90, 91] In every year since 1900, with the exception of 1918, (year of the most severe outbreak of influenza in United States history), CVD accounted for more deaths than any other cause or group of causes of death. While CVD deaths in the

United States decreased by 24.7 percent between 1994 and 2004, the current epidemics of obesity, inactivity, and diabetes are expected to reverse this favorable trend by 2020. If these predictions are correct, this would translate to a decreased life expectancy for men and women, a first in over 100 years.[92] As such, the decision to create a D4 assay targeting markers of CVD was an obvious choice.

We chose to target two markers of CVD in this initial proof of principle of the D4 assay: (1) Cardiac specific-Troponin I (cTnI) in peripheral blood identifies the presence of myocardial damage, which in turn dictates a specific course of patient management.[93] (2) Brain natriuretic polypeptide (BNP) is a 32-amino acid polypeptide secreted by the heart ventricles in response to excessive stretching and the measurement of BNP represents a standard approach to the diagnosis and management of patients with congestive heart failure.[94]

4.2.1 Multiplexed Assay for BNP and cTnI

Optimized capture antibody concentrations and detection antibody printing conditions were used to print arrays as illustrated in Figure 21. Five replicate spots of each capture antibody comprise a single row in the array. There is one positive control row of an anti-murine IgG directed against the detection antibodies. Twenty-four arrays were printed on one slide, and four slides were assembled into a 96 well plate format.

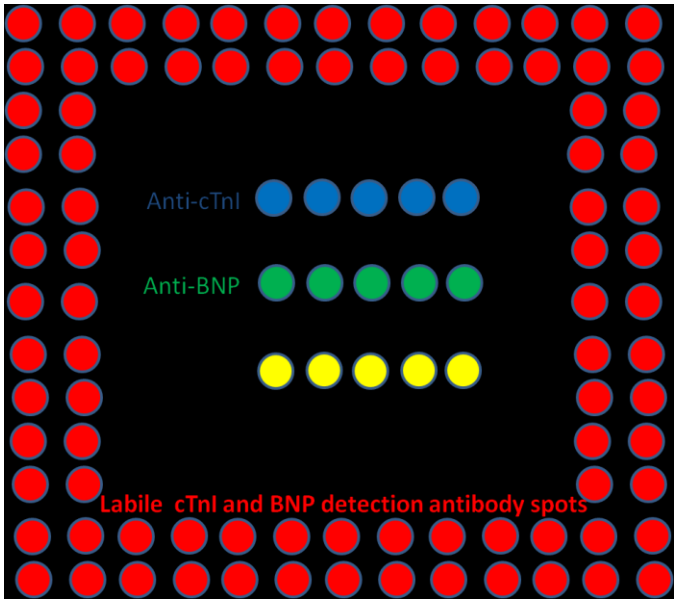

Figure 21 – Cardiac marker array format

Dose response curves covering concentrations from sub-picomolar to nanomolar were generated using target spiked whole chicken blood. Figure 22 illustrates the initial dose response curves produced with the multiplexed assay—the limits of detection for this initial assay were 62pg/mL for cTnI and 125pg/mL for BNP, both of which were well above the limits of detection of current clinical tests for these markers.

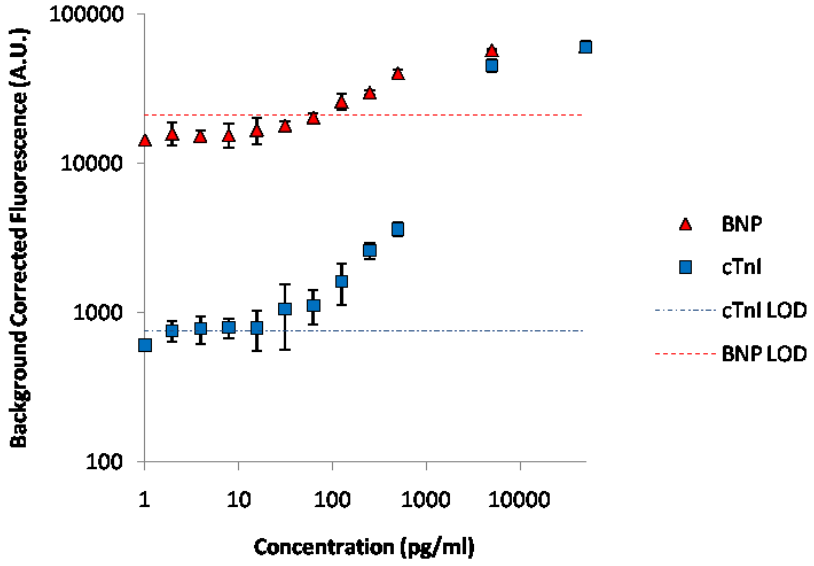

Figure 22: Dose response of multiplexed BNP and cTnI assay. LOD is blank+3SD

The same array format was then used to detect only cTnI spiked blood, or only BNP spiked blood, and the results of these single target assays are shown in Figure 23 and Figure 24. It can be seen from these results that the anti-cTnI antibodies exhibit a high level of cross-reactivity towards the anti-BNP capture spots. Figure 23 shows the results of a single target assay for cTnI in which the fluorescence signal generated at the position of the anti-BNP capture spots (red triangles) varies inversely with cTnI concentration. This highlights the cross-reactivity of the anti-cTnI detection antibodies—as cTnI concentration decreases, the concentration of free anti-cTnI detection antibodies increases, and in the absence of cTnI, these free anti-cTnI detection antibodies bind to the anti-BNP capture spots. This results in the generation of higher fluorescence at the anti-BNP capture spots as cTnI concentration decreases.

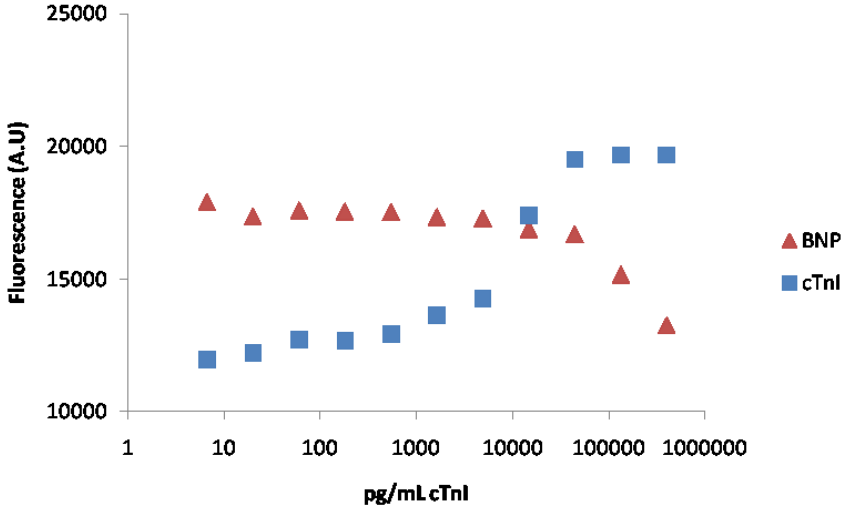

Figure 23: Multiplexed D4 cardiac assay exposed to cTnI dilution series

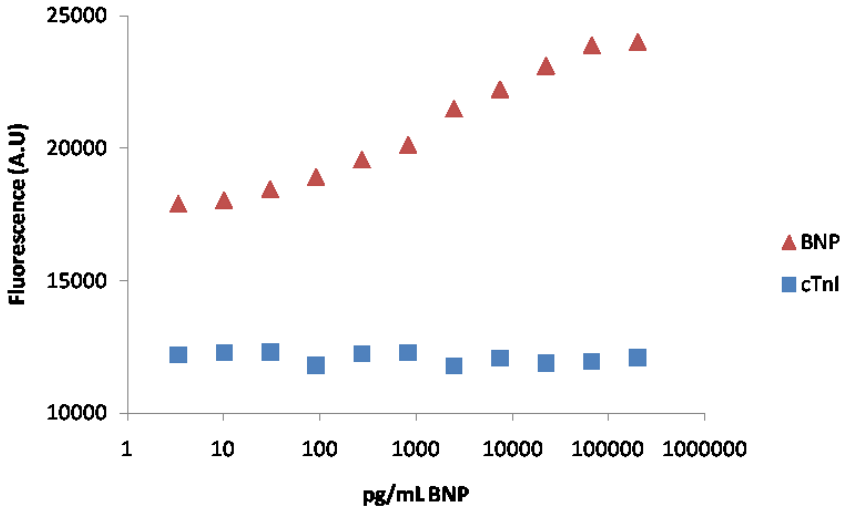

Figure 24: Multiplexed D4 cardiac assay exposed to BNP dilution series

This level of cross-reactivity also limits the sensitivity of the single marker assay for BNP, seen in Figure 21—the "background" signal generated by the cross-reactivity of the anti-cTnI detection antibodies masks BNP binding at low BNP concentrations (BNP binding in the absence of anti-cTnI antibodies is discussed below, see Figure 25). A

number of unsuccessful attempts were made to eliminate the cross-reactivity of the anti-cTnI detection antibodies. Initially, it was assumed that excess conjugation of fluorophore (3.8flours/molecule) to the anti-cTnI detection antibodies led to the high level of cross-reactivity, so attempts were made with antibodies with a lower fluorophore conjugation rate (2.2flours/molecule) as well as with biotinylated detection antibodies—the cross-reactivity was still present however. A separate anti-cTnI monoclonal detection antibody was also evaluated, but without significant improvement.

4.2.2 Single Marker Assay for BNP

Attempted detection of cTnI was concluded after these measures proved unsuccessful, and a single marker D4 assay for BNP was pursued. Figure 25 shows the dose response curve for the single marker assay for BNP. This is the same assay as that shown in Figure 24, however, only anti-BNP detection antibody was printed. With the cross-reactivity interference from the anti-cTnI antibody removed, the limit of detection for BNP improved to 1pg/mL.

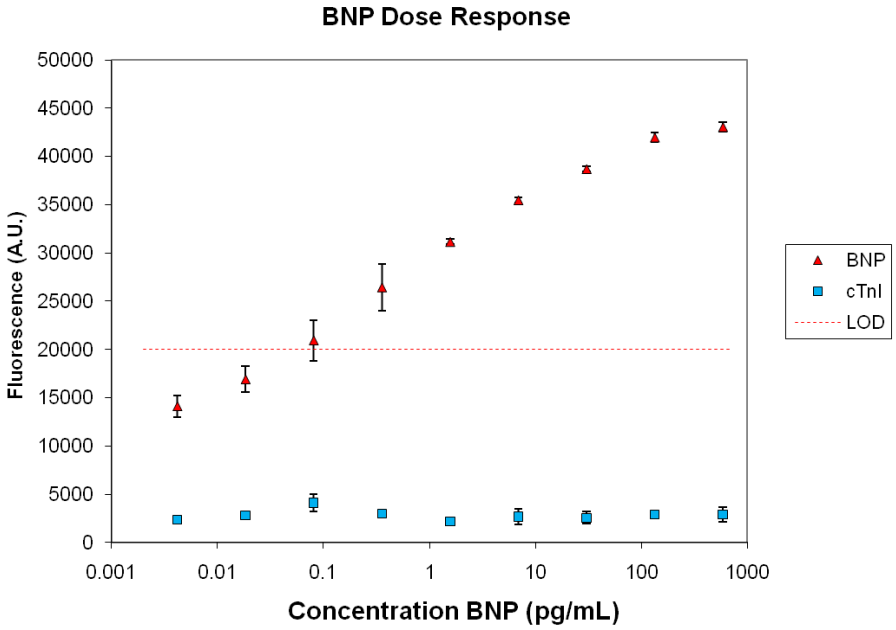

Figure 25: Single analyte D4 assay for BNP. LOD is blank+3SD.

4.2.3 Finalized Single Marker BNP Assay.

Given the promising results of the single marker BNP assay, a larger set of experiments were conducted in order to determine the exact limit of detection of the BNP assay. Array format used is shown in Figure 26.

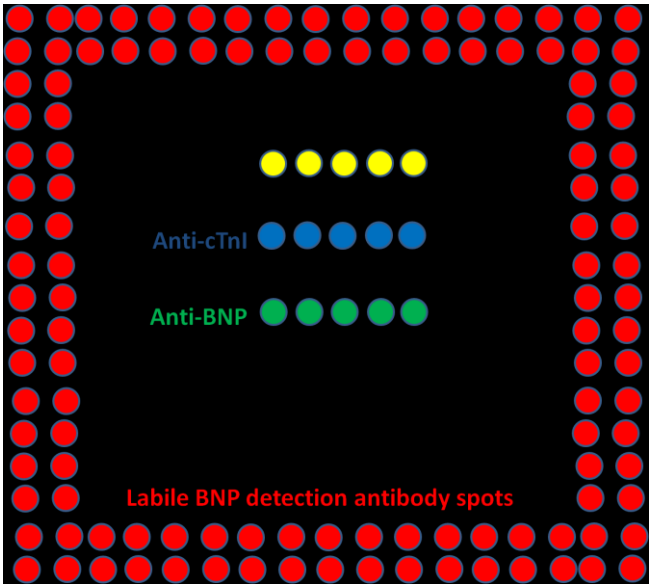

Figure 26: Format of Single Analyte BNP assay. Capture rows consist of: 1) Anti-murine positive control row; 2) Anti-cTnI negative control row; 3) Anti-BNP row. Cy-5 labeled anti-BNP antibody printed as labile spots in outer border.

The experimental set consisted of four replicates of each concentration (spiked into whole chicken blood), assayed on separate slides, along with a total of 16 blanks. In addition, a replicate set of experiments separated from the first set by 22 days was used to assess the shelf life of the D4 assay. Figure 27 shows the dose response curves of assays conducted using slides printed after 1 day and after 23 days of storage at room temperature. Images of the scanned D4 assay from a single set of the full dose response range of concentrations is shown in Figure 28.

The analyte was incubated for 20 min to simulate POC testing conditions. Data was fit with a 5-parameter logistic fit. The fitted curve for the day one assay was used to determine a LOD of 8pg/mL, calculated as the concentration on the fitted curve that

corresponds to the average of 16 blanks plus 3 standard deviations. Importantly, there is no difference in the LOD or dynamic range of the assay, even after storage for 3 weeks. These results are also consistent with previous observations of other investigators that PEG can stabilize proteins under ambient conditions.[95] A long shelf-life under ambient conditions is a useful attribute for point-of-care devices—these printed diagnostic devices will not need to be stored in buffer at 4 ºC, allowing for transport, storage and use at room temperature, which is often essential for use in low resource settings where refrigeration may not be easily available.

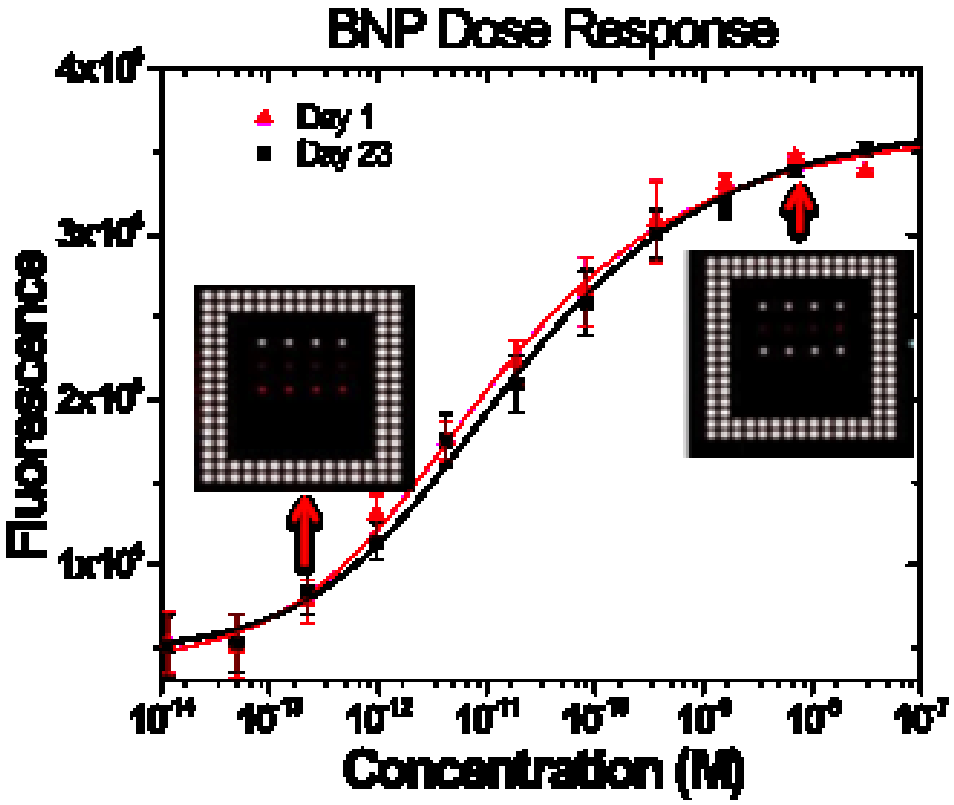

Figure 27: Dose-response curve for a BNP microarray after 1 day (red triangles) and 23 days of RT storage after printing (blue squares). Top row: + control, bottom row: BNP.

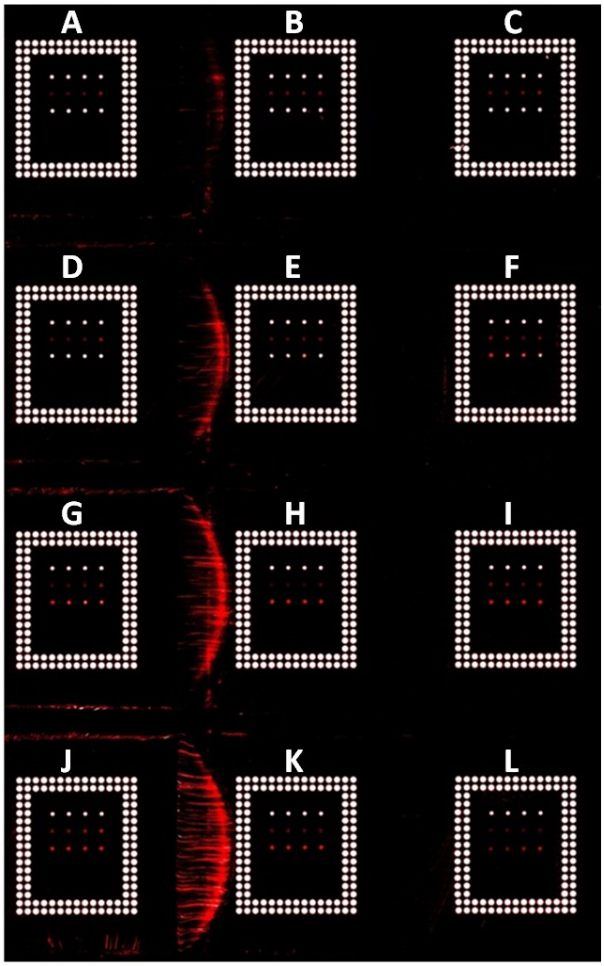

Figure 28: Fluorescence scanner image of BNP dose response. Concentrations as follows: (A)373ng/mL (B)85ng/mL (C)19ng/mL (D)4ng/mL (E)995pg/mL (F)226pg/mL (G)51pg/mL (H)12pg/mL (I)3pg/mL (J)603fg/mL (K)137fg/mL (L)Blank

4.2.4 Commercially available BNP tests

Although further testing is needed, these initial studies suggest that the D4 assay for B-type natriuretic peptide (BNP) should compare reasonably well to these commonly used POC diagnostic tests for BNP:

(1) Biosite Triage System BNP Test (Biosite Diagnostics)—measures BNP concentration from capillary whole blood samples obtained by finger prick. Results are

available in 12-15 minutes. The device has a reported lower and upper detection limits of 5 pg/ml (LOD) and 5000 pg/ml (UDL), respectively.[2] This is a desk-top device, which weighs approximately 0.7 kg. Initial studies claim the test has a 98% diagnostic accuracy at a cut-off value of 80 pg/ml in an urgent care setting.[3]

(2) The Alere Heart Check System (Alere, Stockport, UK) measures BNP concentration from a 15 μl sample obtained by finger prick with results available in 15 minutes using a handheld device.

(3) The Abbott iSTAT Analyser (Abbott Point of Care) measures BNP concentration from a 17 μl sample obtained by finger prick with results available in 10 minutes from a handheld device. The device has a reported lower and upper detection limits of 15 pg/ml and 5000 pg/ml, respectively.[4]

(4) The RAMP 200 Clinical System (Response Biomedical, BC, Canada) measures NT-proBNP from an EDTA whole blood sample, with results available in 15 minutes. The device has a reported lower limit of detection of 18 pg/ml and an upper limit of linearity of 23,450 pg/ml.[5] The product weighs approximately 2 kg.

(5) The Cobas h 232/Cardiac Reader (Roche Diagnostics, Burgess Hill, UK) measures NT-proBNP from a 150 μl sample of heparinised venous blood with results available in 12 minutes. This handheld device has reported lower and upper limits of detection of 60 pg/ml and 3000 pg/ml, respectively.[6]

The 8pg/mL LOD of the D4 assay compares well with most of these commercial POC tests for BNP. Furthermore, a major advantage of the D4 assay is that it can decouple the test from the instrument because all the reagents are printed on-chip and there is no need to separate blood cells prior to analysis, whereas many of the cartridge/microfluidics based tests have to be performed in a setting where the analyzer is available (e.g., doctors office or home), as they require separation of the blood components and release of detection reagents from a sealed pouch or reservoir. In contrast, the D4 assay is closer to a LFA in its design in that it can be used when and where needed, when combined with a visual read-out or a modified cell phone. This enables it to be administered in an ambulatory setting (on the battle-field, sports arena, or scene of accident) similar to an LFA, with the added benefit of being multiplexed and quantitative.

4.3 Multiplexed D4 Assay for IL-6 and PSA

Because a successful multiplexed D4 assay was not realized with the chosen cardiovascular disease markers, two additional markers were chosen to demonstrate the multiplexed capabilities of the D4 assay: 1) IL-6 and 2) PSA. IL-6 was chosen in order to compare results of the D4 assay with that of the first generation assay for IL-6 described in section 3.2.2. PSA was chosen because of the potential need for high-sensitivity detection of PSA, described subsequently.

4.3.1 Need for Highly Sensitive PSA assay

The limited sensitivity of currently available prostate specific antigen (PSA) assays hinders early detection of the recurrence of prostate cancer in patients following radical prostatectomy (RP) surgery; in 2009, there were approximately 86,000 RPs performed in the US.[96] This is because post-RP, PSA levels are typically undetectable due to the fact that RP surgery removes the tissue responsible for PSA production. However, several studies have recently shown that a slow increase in blood PSA level following RP is an indication of cancer recurrence.[97-102] However, current FDA approved PSA tests, with a limit-of-detection (LOD) of only 100pg/mL ($3x10^{-12}$ M),[103] are too insensitive to catch this slow increase in a timely fashion. The ability to measure lower PSA levels post-RP can improve the treatment of post-RP prostate cancer patients through a more accurate assessment of patient prognosis and response to treatment, as well as allow targeted secondary therapy. [104-107] Motivated by this rationale, our goal is to use the D4 platform to develop a sensitive PSA assay capable of detecting the recurrence of prostate cancer in patients who have undergone RP.

4.3.2 Multiplexed POC D4 Assay for IL-6 and PSA

Dose-response curves in Figure 29 were produced by analyzing whole chicken blood spiked with human IL-6 and/or PSA—ten microliters of blood at each concentration was added to the chip and incubated for 20 minutes, followed by a 1mL squirt bottle rinse step as shown in Figure 19. The limits of detection (blank + 3SD) for

this multiplexed D4 assay are 15 pg/mL for PSA and 2pg/mL for IL-6. In contrast, an optimized ELISA with these Abs that takes 100 μL of serum and 5 hours to complete yields detection limits of 30pg/mL for PSA and .7pg/mL for IL-6. These ELISAs are not multiplexed nor can they be carried out from whole blood. These results show the power of the D4 assay to provide multiplexed, ELISA-like or better sensitivity from just 10uL of whole blood in a POC setting.

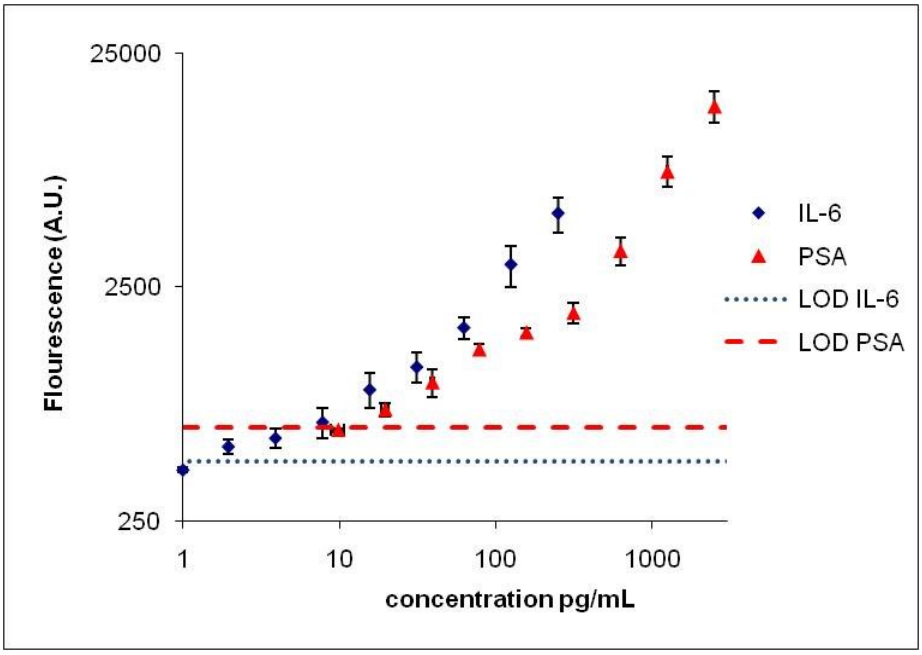

Figure 29: Results of multiplexed D4 assay for human PSA and IL-6 spiked into chicken whole blood. LOD is blank + 3SD

4.4 Materials and Methods

4.4.1 Slide preparation

Slides were coated with POEGMA as described in section 3.4. A slide imprinter (The Gel Company) was then used to imprint POEGMA coated slides with a thin pattern

of hydrophobic wax. The stamp was first immersed in a bath of wax heated to approximately 60 degrees Celsius and then lifted out of the wax and placed in contact with the slide for 1 second.

4.4.2 Microarray fabrication

All antibodies used in our experiment were reconstituted in 1x PBS solutions and passed through 0.2 μm filters prior to printing of microarrays. 15-20 μL of capture antibodies at a concentration of 0.5-1 mg/mL were pipetted into a 384 well microplate. Next, a 15-20 μL solution consisting of 0.5-1 mg/mL fluorescently tagged detection antibodies and 1 mg/mL polyethylene glycol excipient (MW 11.6K) was prepared and pipetted into a separate well of the microplate. The microplate was then centrifuged at 2000 rcf for 30 seconds to ensure solution had settled in the bottom of the microplate wells.

Next, slides coated with ~30 nm poly(oligoethylene glycol methacrylate) (POEGMA) were placed on the printing deck of a Perkin Elmer Piezorray Flexible Non-contact Microarraying System. The Piezorray is a versatile inkjet printing instrument which can array microdrops of ~300 picoliters with high fidelity (better than 5 μm spatial resolution), allowing precise control of microarray geometry. Each spot printed in our arrays were ~150 μm in diameter. The "stable" capture antibodies were first printed in a linear 1x4 array, with each spot spaced 300-500 μm apart, depending on the experiment. Next, fluorescently labeled detection antibodies mixed with PEG excipient were printed

as in the geometries described in the main text of this dissertation. Between each sample, Piezorray tips were thoroughly purged with HPLC grade water, sonicated in 1% tween/PBS solution, and purged again with water to ensure removal of residual sample from the previous run. All printing was performed under ambient conditions. Slides were then vacuum desiccated overnight.

4.4.3 Diffusion assay

D4 arrays on POEGMA were incubated with 10 to 100 microliters of analyte-spiked PBS, heat-inactivated fetal bovine serum, heparinized whole chicken blood, or a drop of blood obtained directly from a fingerstick for 5 to 30 minutes under ambient conditions. The arrays were then washed with either 0.1% Tween 20 in PBS using a plate washer or with several drops of saline solution in order to displace the analyte sample prior to imaging. Arrays were imaged using an Axon Genepix 4200 scanner utilizing a 635nm solid state laser and Cy5 filter set.

5. Finalizing the D4 Assay

Previous chapters have demonstrated the optimization of the D4 biointerface, and all data shown up to this point was generated by using chips in which the blood sample was exposed to the environment (see Figure 3D)— i.e., was not sealed or contained—and assays required a final rinse step for removal of the blood cells (see Figure 3E), while a fluorescent slide scanner was used to image microarrays. However, in order for the D4 assay to provide results at the point of care, the blood must be contained, the final rinse step must be eliminated in order to reduce the steps an end-user will be required to perform, and a portable, low cost method of quantifying microspot intensity must be included in the system. Addressing these aspects of the assay format is necessary to create a true point of care test that has no user intervention and is comparable to a lateral flow assay. Preliminary work towards these two goals is presented here.

5.1 Solving the blood containment problem

In order to contain the blood sample, the D4 chip was redesigned. The second generation D4 chip consists of a coverslip wherein the central region is printed with the capture spots, surrounded by labile spots of the detection reagents, similar to the first generation chip. Adhesive is applied and a second coverslip is used to cover the printed spots of capture and detection antibodies such that the spots are now contained within a central channel exposed on both ends, with the analytical core of the D4 assay contained

in the center of the channel (Figure 30A). The channel width can be controlled by the area of the chip that is covered with adhesive and the amount of adhesive applied controls the height of the channel. This enables channel volumes of just a few microliters of blood, and is consistent with a volume that can be easily obtained from a finger stick. Channel dimensions were selected to also provide enough capillary force so that when a drop of blood is held up to one of the two ends of the channel, it is wicked into the channel by capillary action (Figure 30B –C). Furthermore, the interfacial tension of the blood also keeps it contained within the chip (Figure 30D). This self-loading and self-sealing design completely contains the blood within the chip.

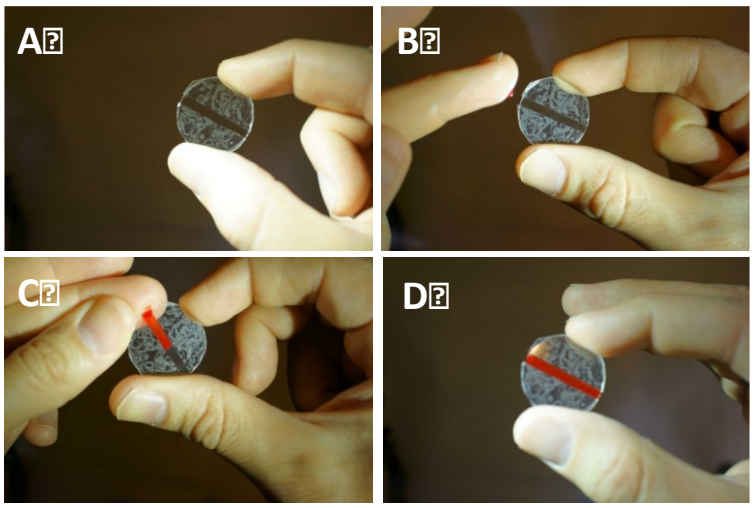

Figure 30 Example of a second generation D4 chip (A). The antibody microarray is printed on the bottom coverslip of the in the center of the channel. Illustration of how blood is loaded into the central channel and is retained within the channel by capillary action (B-D).

5.2 Solving the final rinse problem

In the original design of the D4 chip, the fluorescence was measured in reflectance mode on a microarray slide scanner, which requires that blood is removed from the chip by a final rinse. Wash steps are undesirable in POCTs because they require user intervention, which makes a POCT with a rinse step less robust than one without any user intervention steps. To eliminate the final rinse step, an optical detector was designed (described in section 5.3) such that both the excitation of fluorescence and the imaging of fluorescence occurs through the bottom coverslip so that optical interference from the blood sample is minimized in order to eliminate the final rinse step and image the array while the central channel is still filled with blood.

The unique geometry of the D4 biointerface (Figure 31) makes it possible to preferentially excite labeled detection antibodies involved in antigen detection while minimizing the excitation of unbound detection antibodies present in the blood sample. This is possible because of the two tier structure of the polymer brush coating on the surface of the D4 chip. A high density polymer brush coating at the substrate surface prevents all large biomolecules and cells from approaching the substrate surface. This high density surface coating gradually progresses to a lower density coating, which provides sufficient free volume for the immobilization of capture antibodies under dehydrating conditions. Upon rehydration, the lower density polymer brush corona present at the coating/blood sample interface provides a partial barrier to the presence of

cells and large, unbound biomolecules, including the labeled detection antibody. Only those labeled antibodies which diffuse into the low density corona and become tethered to the surface via antigen binding are capable of persisting within the polymer brush layer, as the substantial excluded volume of the low density corona effectively limits the presence of unbound molecules.

This unique geometry of the biointerface traps the labeled detection antibodies involved in antigen detection within the optically transparent polymer brush layer. Unbound detection antibodies remain dissolved in the optically adsorbing and scattering blood sample. Excitation light illuminates the bound detection antibodies within the optically transparent polymer brush layer, but does not reach unbound detection antibodies in solution due to the rapid dissipation of excitation light by the blood sample.

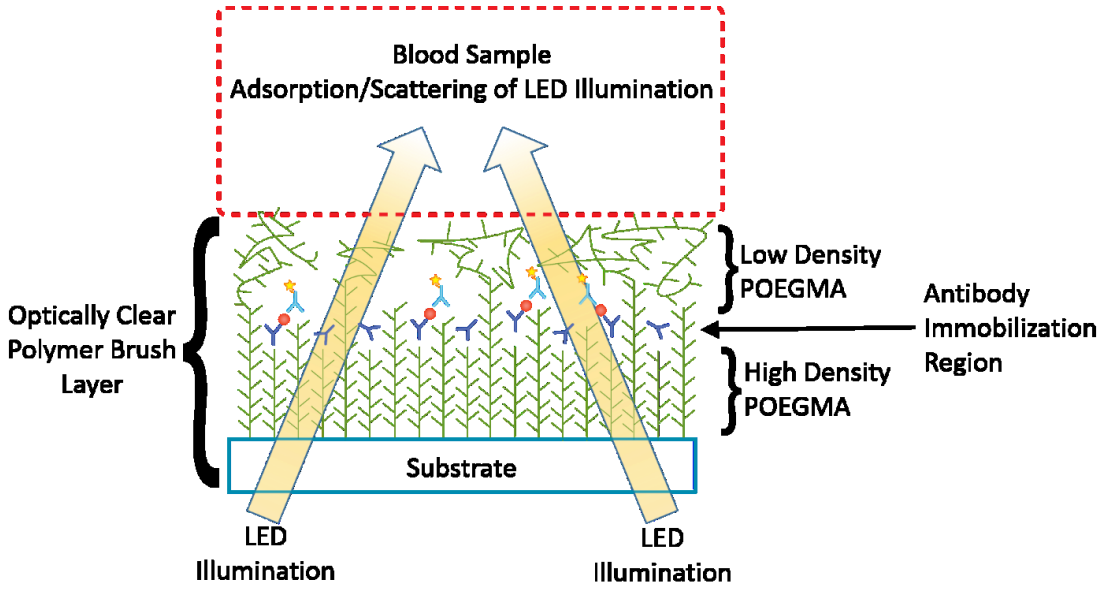

Figure 31: Geometry of the D4 biointerface.

5.3 Design of a cell phone compatible optical detector with visual backup.

The optical detector was designed with these requirements in mind:

(1) The detector should be small and light-weight, so that it can be easily carried in a user's pocket, thereby unchaining the patient from the detector. This is in stark contrast to the design of current point of care tests (e.g., iSTAT and Biosite) which are significantly larger, and are more suitable for caregivers than a patient. (2) The optical detector should be low cost and easy to manufacture at high volumes using widely accessible and low cost manufacturing technology (3) The detector should be compatible with a range of smart phones. (4) The optics should not require any alignment or adjustment. (5) The detector should be able to quantify the fluorescence signal in the

presence of blood. (6) The detector should have visual backup to allow readout of qualitative results, if a smart phone is not available.

The design of the detector is shown in Figure 32. The casing of the detector was fabricated on a Stratasys 3-D printer in ABS thermoplastic as two separate pieces: a lid and body. The lid contains an insert for the battery and has threads to allow it to be screwed into the body of the detector. The body has 4 cavities into which LEDs can be inserted and provide illumination of the test array at a 45º angle, and a frame into which the band-pass filter can be inserted. Assembly of the detector is simple: after fabrication of the two printed pieces, the bandpass filter is inserted into its holder, and four LEDs are inserted into their prefabricated cavities and wired to allow contact with the lid when it is screwed on to the detector. Assembly is complete after a 10X magnification lens is added, a battery is inserted into the lid, and the lid is screwed into the body of the detector. Finally, a concentric magnetic ring is glued into the rim of the lens of the detector.

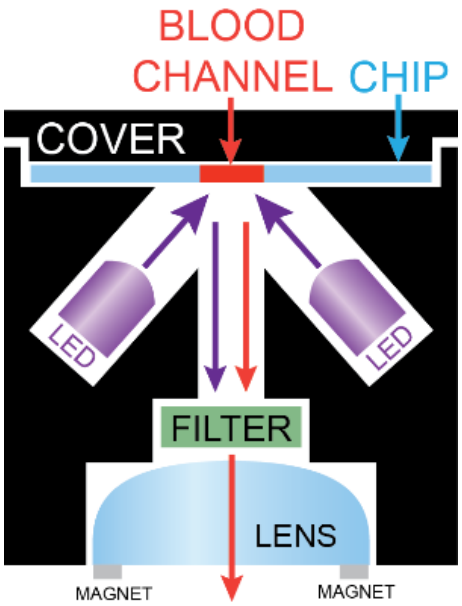

Figure 32: Cutout schematic of detector design. Backside illumination and collection reduce optical interference from blood.

Use of the detector is equally simple (Figure 33). The lid is unscrewed revealing a slot for the blood-loaded chip to be placed, such that the coverslip with the printed antibodies is on the bottom (away from the lid). With the chip placed in this configuration, the fluorescent spots in the D4 array are illuminated from below by the LEDs. Only the emitted fluorescence passes through the band pass filter placed between the chip and the lens of the detector. The spots are magnified 10X by the lens and an image of the array is digitally captured by the smart phone camera. The detector and smart phone optics have a built-in magnetic self-alignment: a concentric magnetic ring is glued both on the lens of the detector and around the lens of the smart phone, which magnetically aligns the optics of the two devices.

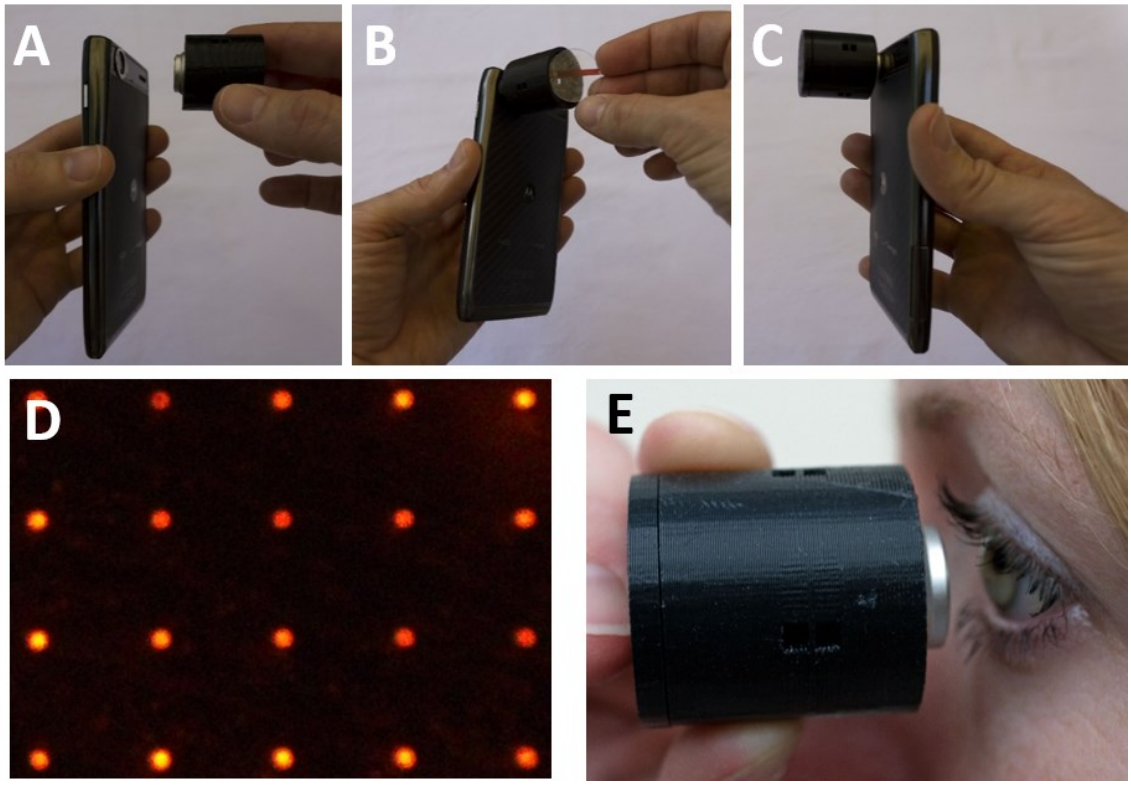

Figure 33: Detector workflow and readout. (A) Magnetically connecting detector to phone. (B) Inserting chip into detector. (C) Chip ready for imaging with phone camera. (D) Actual phone image of test microarray after addition of blood. (E) Direct microarray viewing.

5.4 Quantum Dot Labels

Modern immunoassays typically utilize chromogenic, fluorescent or electrochemical effects to transduce antibody-antigen binding into a measureable output.[108] Fluorescence detection is generally preferred because: (1) background fluorescence is generally weak or nonexistent; and (2) fluorescence signaling relies on well-established and generally applicable chemistry. However, while both fluorescence and electrochemical detection are amenable to multiplexed platforms, both typically

require relatively sophisticated data capture and analysis platforms. Chromogenic assays, which are technologically simpler than the other two types of detection, are already in common practice for pregnancy testing based on human chorionic gonadotropin.[109] Unfortunately, most target biomarkers are not present in concentrations sufficient for direct chromogenic detection. To resolve this problem, many complex and expensive methods for signal amplification have been developed.[110-113] While these strategies have demonstrated colorimetric gains by factors of over 100, this amplification is not sufficient for many applications at the POC and in low-resource settings.

As demonstrated in previous chapters, we have focused on fluorescent signal generation. The majority of fluorescence detection systems rely on epifluorescent illumination, which typically requires side illumination, relatively expensive band pass excitation and emission filters, and a dichroic mirror. In an attempt to simplify detector design, the use of commercially available streptavidin coated fluorescent quantum dots is being pursued. The use of quantum dots allows us to perform measurements in transmission mode, use less expensive cut off filters, and create a multi-color assay with a single inexpensive LED illumination source.

Quantum dots exhibit a large Stokes shift—excitation and emission wavelengths can be separated by 200nm or more, compared to a typical 20nm for organic fluorophores. This large Stokes shift makes it possible to design a less complex, less

expensive detector due to the fact that excitation and emission wavelengths can be separated much more efficiently. For instance, when coupled with a low cost ($1) UV light emitting diodes that provide a narrow band of excitation light, the only filter necessary for fluorescence detection is a less expensive longpass emission filter (as opposed to a bandpass filter). In addition, the large Stokes shift also allows for transmission measurements, as excitation wavelengths can be efficiently blocked from reaching the detector without significantly affecting emission wavelengths, which simplifies the light path when compared to epifluorescence illumination.

Quantum dots also resist photodegradation to a much greater extent than organic fluorophores, which relaxes the light exposure limitations that a pre-printed assay chip can withstand and also limits the effects of photobleaching during signal acquisition. Finally, the use of quantum dots allows for the development of a multicolor assay using a single, unfiltered excitation source.

These advantages led us to explore the use of quantum dots labels for the D4 format described herein. As an initial proof of principle, a test array of quantum dots was printed in the central channel of a D4 chip. Blood from a fingerstick was then added to the chip as shown in Figure 30, and the test array was imaged with the device shown in Figure 32 and Figure 33. The resulting image in Figure 33D suggests that this approach may prove useful and merits further development. In addition, imaging of the

test array prior to the addition of blood is shown below, as is an example of multi-color detection with the cell phone compatible device described above.

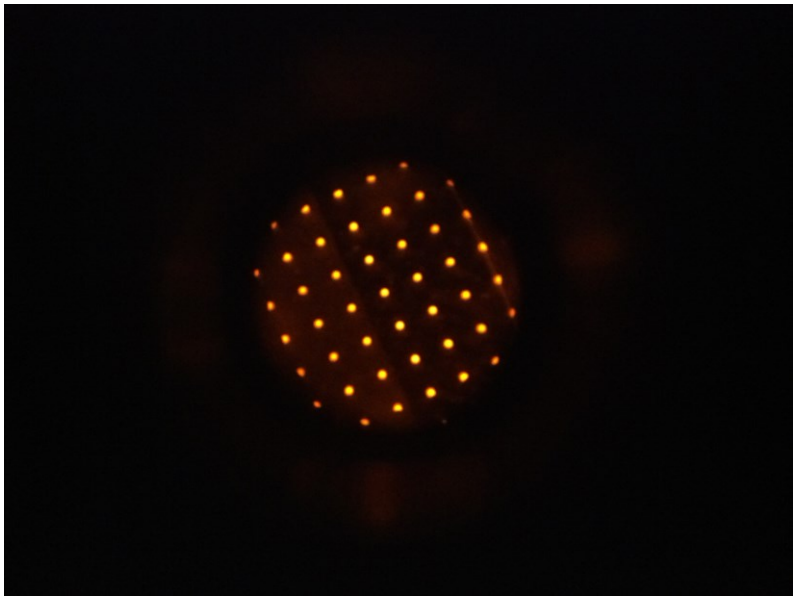

Figure 34: Image of a test array printed within the central channel of a D4 chip prior to addition of blood and imaged with the cell phone compatible device described in Section 5.3

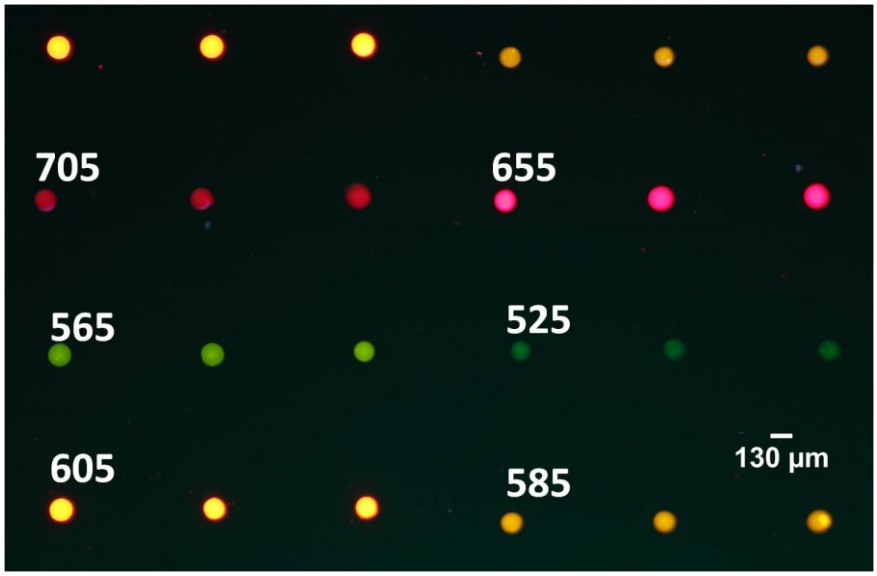

Figure 35: Demonstration of multicolor imaging of a test array printed using quantum dots of various emission wavelengths (labeled with the manufacturer quoted emission wavelength for each type of quantum dot used in array).

5.5 Summary

To be useful in a field use setting—doctors' office, home care or clinical test site—a diagnostic test should meet the World Health Organization's ASSURED criteria. The acronym ASSURED stands for: A = affordable; S = sensitive ; S = specific ; U = user friendly (simple to perform in a few steps with minimal training); R = robust and rapid (results available in less than 30 minutes); E = equipment free; D = deliverable to those who need the test. With continued development of the modifications described in this section, we believe the D4 point of care test has the potential to meet the ASSURED criteria by applying novel biointerface science and technology to the design of an assay that is markedly different than any other POCT currently in use.

A = affordable. The D4 POCT leverages the increasing ubiquity and rapidly lowering cost of smart phones, which are increasingly prevalent in LMICs. This

significantly reduces the largest upfront cost for most POC assay systems: the cost of the dedicated detector and signal analyzer.

S = sensitive. Current data, shown in Preliminary Studies, suggests that we can already meet the performance metrics of sandwich immunoassays carried out in a centralized lab setting. Hence, the optimized D4 POCT should yield highly sensitive results in <20 minutes that are comparable to or better than ELISAs and sandwich fluoroimmunoassays that take ~4-6 h to complete in a centralized laboratory.

S = specific. Because the test relies on an antibody sandwich that is highly specific, as long as an antibody pair that is specific for an analyte is available that does not cross-react with other assay components, we can design a D4 POCT for a disease of interest. We have found that for a single analyte assay, specificity is never a problem. However, for dual analyte assays, it is important to screen available antibody pairs to ensure that the pairs are not cross-reactive with each other.

U = user friendly (simple to perform in a few steps with minimal training). The D4 POCT simply requires a finger stick and touching the edge of the D4 chip to the drop of blood, which loads the blood into the chip by capillary action. Capillary action also keeps the blood confined to the central channel, so that the chip is both self-loading and self-sealing. After waiting a prescribed duration of time, which ranges from 5 to 20 minutes depending upon the desired sensitivity required for diagnosis, the chip is inserted into the detector, and the detector is connected to a smart phone camera. The magnetic ring on the front of the detector and a matching adhesive backed ring attached to the smart phone self-align the optics of the detector and smart phone camera, and the

user then takes a picture of the array. The smart phone app then converts the picture into a diagnosis.

R = robust and rapid (results available in less than 30 minutes). The test appears to be rapid, as preliminary studies have shown it is possible to attain picomolar sensitivity with 20 minute incubation times. It is also robust, as the POEGMA coating eliminates non-specific protein adsorption and cell adhesion and thereby removes the largest source of assay uncertainty. The chips also do not require a cold-chain and can be stored at room temperature for a month or more.

E = equipment free. The D4 POCT is almost equipment free. It has a small detector, the size of a jewelers' eye-glass that magnetically attaches to a smart phone and enables one to take a digital photograph of an antibody microarray. Alternatively, if a smart phone is not available, the detector can be held up to the eye and the spots can be visualized through the built in lens in the eyepiece (see Figure 33).

D = deliverable to those who need the test. The chips cost cents to make by inkjet printing, and do not require a cold chain, so they can be stored without hydration or refrigeration. Similarly, the detector prototypes cost ~$30 to make by 3-D printing, but a cost close to $5 should be possible when manufactured at large volume. There are no moving parts and the detector can be powered by a watch battery or by the smart phone's USB port. Hence, the test has a number of advantages that should make it deliverable in a LMIC setting. While it will likely be preferable to use a smart phone to capture images of the spots in the microarray and convert to concentrations by an App loaded on the smartphone, it is certainly not imperative. The detector can also be read visually through the eye-piece that attaches to the smart phone, and because we plan to

print a calibration row of spots of the analyte as a dilution series on the D4 chip (see section 6.1 below), we hope to enable visual determination of the concentration of the unknown sample by interpolation.

5.6 Materials and Methods

5.6.1 Chip Fabrication

5.6.1.1 Polymerization

25mm round #2 coverslips (Ted Pella) were loaded into a custom teflon coverslip holder and cleaned with a 1:1 HCl:Methanol solution for 30 minutes and then rinsed three times with ultrapure water. After cleaning, coverslips went through the same silanization, initiator deposition, and polymerization process as that described for slides in section 3.4.1 through 3.4.3, with the exception that each process step took place in 50mL Teflon beakers (Ted Pella) instead of 400mL glass staining jars. 25mm square silicon wafer substrates (University Wafer) were processed alongside coverslips and POEGMA layer thickness was measured using an M-88 ellipsometer (JA Woollam).

5.6.1.2 Printing

Solutions of streptavidin coated quantum dots (Invitrogen) with peak emmissions at 525nm, 565nm, 585nm, 605nm, 655nm and 705nm were passed through a .2 micron centrifugal filter (Amicon) and resuspended at a concentration of 1 micromolar in PBS (Sigma). 20 microliters of each solution of quantum dots was added to a single well in a 384 well plate (VWR). 6 microliters of each solution was aspirated using a Perkin Elmer Piezorray tuned to produce 300pL droplets. Individual 300pL

droplets were arrayed onto the surface of POEGMA coated coverslips at a spacing of 900 microns.

5.6.1.3 Assembly

Arrayed coverslips were loaded into a custom fabricated coverslip holder with channels to guide placement of double sided adhesive tape. Two pieces of 100 micron thick adhesive were applied to the chip surface on either side of the array located at the center of the coverslip such that a 25mm by 2mm channel containing the central array was formed. A second POEGMA coated coverslip was then added to form the top surface of the chip using the same coverslip holder to guide alignment of the two coverslips.

5.6.2 Detector Fabrication

CAD software was used to design the detector housing, which was printed using a Stratasys Dimension 1200ES. Four 5mm light emitting diodes with 30mW radiant power and a 15 degree viewing angle were inserted into the detector body, wired in parallel, and connected to two CR2450 batteries contained within the detector lid. An LED emission peak of 380nm with a 15nm FWHM spread was observed by coupling the LED emission light into a fiber optic light guide attached to an Ocean Optics USB4000 spectrophotometer. A 12.5mm longpass emission filter (Edmunds Optics) with a cutoff wavelength of 500nm was added to the detector housing and press fit into place. A magnetic cell phone macro lens (Amazon.com) with an approximate focal length of

20mm was press fit into the detector housing directly adjacent to the emission filter. The camera of a Samsung N9000 cell phone was modified with a matching 10mm diameter adhesive magnetic ring (provided as part of the macro lens kit) and used to image the quantum dot arrays with the phone's native camera application.

6. Design of next generation of D4 chips

6.1 Self-Calibrating Chips

The analytical robustness and performance of the D4 platform could potentially be enhanced through the development of a self-calibrating scheme in which a dilution series of target is printed on the chip as a row of positive control capture spots (Figure 36). Signal generation at these control spots will signify a viable assay by verifying activity and diffusion of the detection reagents. In addition, by varying the concentration of target within these control spots, there will be a signal gradient across the spots that can be used to normalize fluorescence intensities and reduce inter-assay variability. This control gradient can also be compared to signal generated at the capture antibody spots, which will aid in quantification of target levels and reduce sampling variables such as volume of blood added to the chip, blood viscosity, incubation temperature and time to measurement. In essence, the spot intensity gradient of the positive control spots will provide a reference signal, similar to a dose-response curve, that will serve as an internal calibration for each chip.

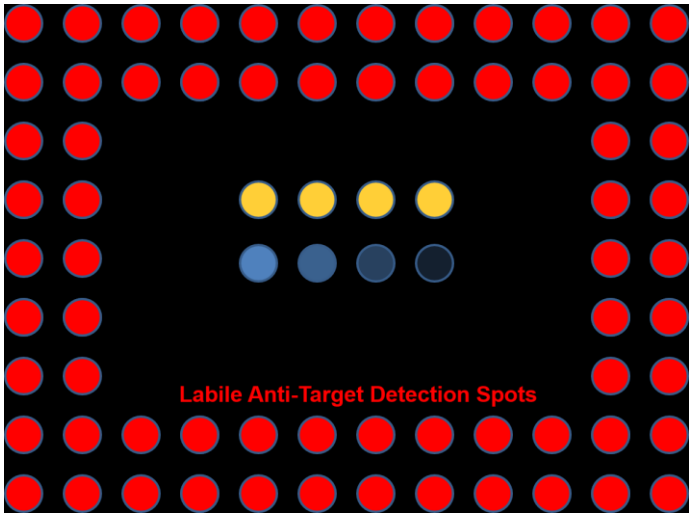

Figure 36: Format of self-calibrating D4 microarray. The signal gradient produced by varying target concentraton within the +control spots serves as an internal calibration standard.

6.2 Soluble detection reagent position

In traditional lateral flow immunoassays (LFA), analyte solution dissolves soluble detection reagents prior to reaching test lines of capture antibodies. This is necessary because the flow stream in an LFA is in one direction only, and therefore the detection reagents must be dissolved in the analyte solution prior to reaching the capture antibodies. As such, the traditional LFA format allows detection antibodies to bind antigen prior to antigen-capture antibody binding, and therefore the potential exists for antigen-detection antibody binding to block antigen-capture antibody binding. Using a carefully matched pair of monoclonal antibodies minimizes this issue, but can significantly increase cost.

The diffusion based design of the D4 format does not require the upstream placement of detection antibodies, and it may be possible to increase sensitivity by

allowing the analyte solution to contact capture spots prior to detection spots. This should allow antigen to initially bind to capture spots without any interference from detection antibodies, as the detection antibodies will only contact the capture spots through the diffusion that occurs after the capture spots have been exposed to the analyte solution.

Figure 37 illustratres a test format that could be used to test this hypothesis, which involves alternating the position of two separate arrays within the central channel of the chip: 1) An array composed of anti-target capture spots (yellow) and target calibration spots (blue), and 2) An array of soluble anti-target detection spots (red).

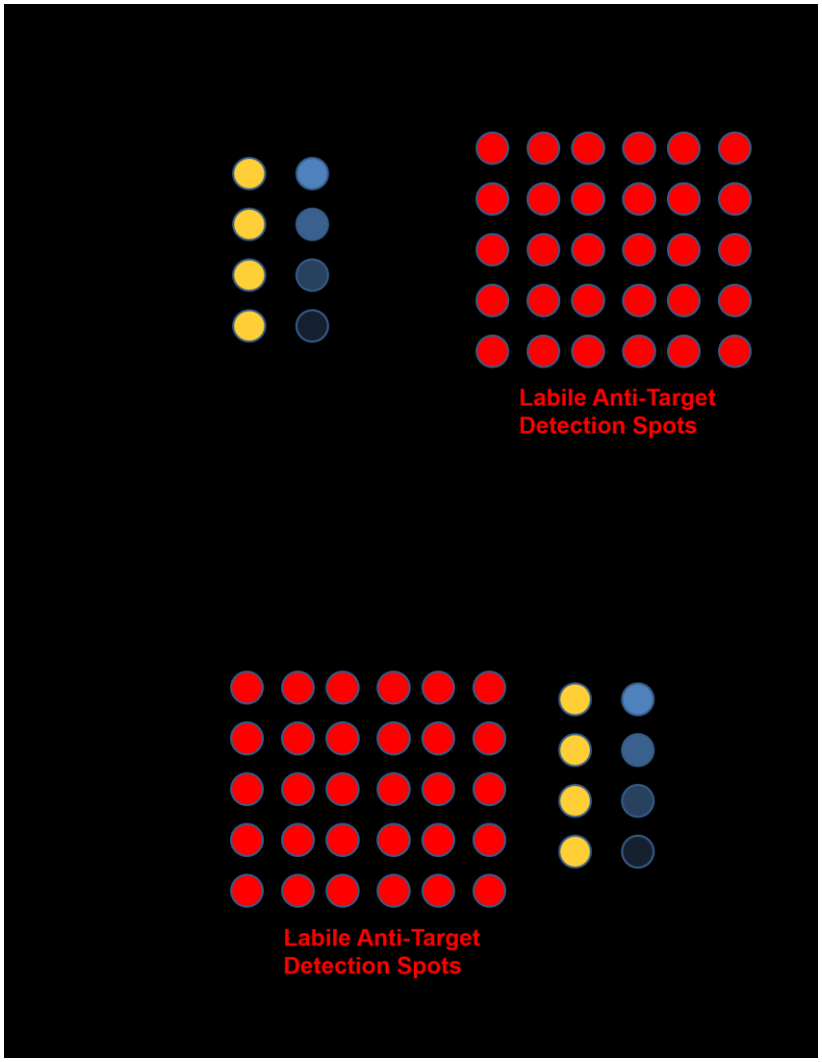

Figure 37: Test array format. Two separate arrays will be printed: 1) An array composed of anti-target capture spots (yellow) and calibration spots (blue), and 2) An array of soluble detection spots (red). The order in which these two arrays are exposed to analyte solution will be alternated—blood initially contacts capture spots first in panel A, and detection spots first in panel B.

6.3 Effect of diffusion distance on D4 assay.

Positioning the soluble detection spots as closely as possible to the capture spots has the potential to improve the D4 assay format in two ways: (1) assay reaction time will be decreased if each capture spot is surrounded by multiple soluble detection

reagent spots in close proximity, and (2) this geometry will be capable of providing higher local concentrations of dissolved detection reagents around each capture spot and thereby reduce the amount of detection reagent that must be printed on-chip. An array format to test this hypothesis is shown in Figure 38.

Figure 38: Test array format. Each stable capture spot is surrounded by labile detection spots in order to reduce diffusion distance of detection antibodies.

This geometry provides shorter diffusion distances and therefore potentially faster labeling of captured antigen than the previously described geometry in which the capture spots are surrounded by concentric rings of labeled detection antibody. To test this hypothesis, the array in Figure 38 should be exposed to a dose response of antigen and compared to the standard D4 assay shown. Assuming the figures of merit are equivalent to or better than the standard D4 assay, a time course video of the assay can

be used to assess the degree to which incubation time can be shortened while still retaining the performance metrics of the standard D4 assay.

While a shortened assay would be advantageous, it is also useful to determine how this geometry can potentially decrease assay cost by reducing the amount of detection antibody printed on the chip. In this case, local concentrations of detection antibody around each capture spot should be higher during detection spot dissolution. This higher local concentration due to spot proximity should allow decreased amounts of printed detection antibody to produce the same local concentration around each capture spot as is achieved with the larger amounts of detection antibody that are printed in the first generation D4 format. By systematically decreasing the amount of detection reagent printed in each detection spot, the minimum amount of detection reagent necessary to produce figures of merit equivalent to the standard D4 assay will be determined.

In addition to the possible advantages discussed above, this geometry should provide each capture spot with a more uniform exposure to detection antibody during detection spot dissolution, as each capture spot is located the same distance from the nearest detection spots. In conclusion, this geometry should be evaluated to determine if a useful reduction in assay time, total printed detection antibody amounts, and/or assay variability is observed.

7. Future Directions

7.1 A competitive binding assay for single-step detection of microRNA sequences

This concept (Figure 39) is similar to a competitive immunoassay, however, the method of delivery of the labeled/competing target is different—in this format, the labeled target is not spiked into the analyte solution, but is instead hybridized directly to the probe prior to spotting. As such, this format relies on microspots of probes that have been hybridized to a labeled target prior to spotting. By designing the sequence of this labeled target to include a number of non-complementary bases, there should be a displacement of this pre-hybridized, partially-complementary labeled target by any target present in an analyte solution (target present in the analyte solution does not contain any mismatched bases, and therefore hybridizes with higher affinity to the probe sequence). In this format, a decrease in microspot signal intensity is used to quantify target in the analyte sample. Ideally, this method would avoid an RNA purification step. However, even if RNA purification is required, this method still has the potential to eliminate reverse transcription, labeling, and/or PCR amplification.

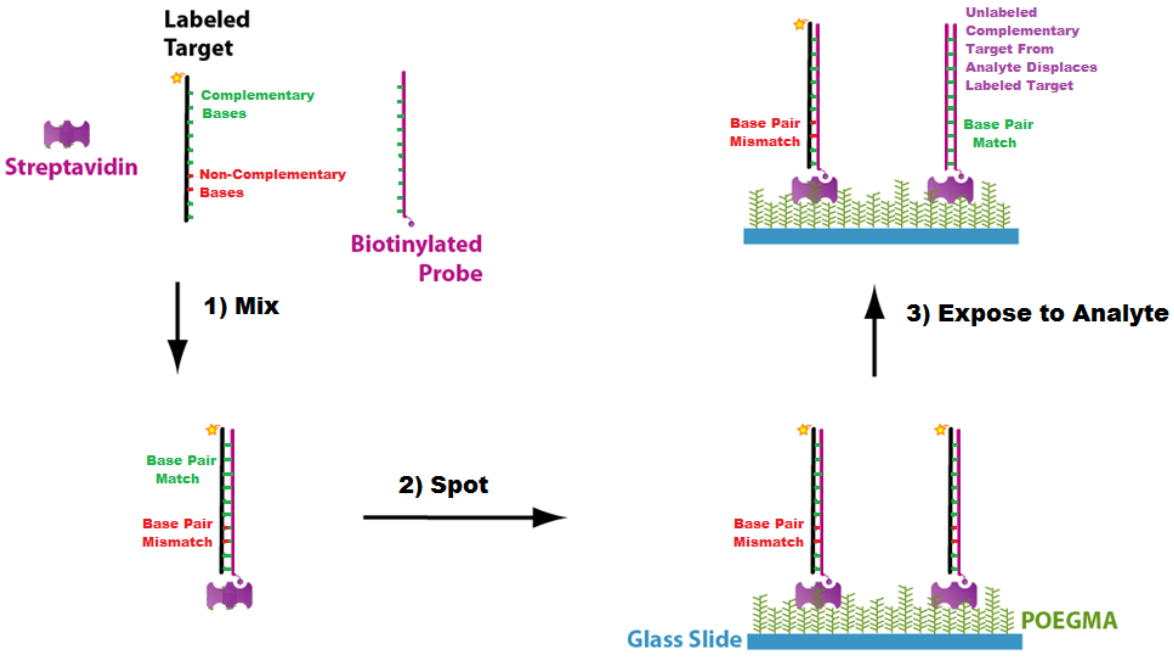

Figure 39: A competitive binding assay for single-step detection of microRNA sequences

The basic uncertainty of this method surrounds: 1) The ability of a complementary target (from a patient sample) to bind to a probe sequence which is already partially hybridized to a labeled sequence that contains a number of non-complementary bases; 2) How many non-complementary bases on the pre-hybridized, labeled target are needed to obtain a quantifiable decrease in spot intensity from a given concentration of unlabeled, complementary target, and is the corresponding limit of detection physiologically relevant (i.e. is the physiologic concentration of the target quantifiable by these methods); 3) How many non-complementary bases can occur on the pre-hybridized, labeled target before specificity is lost (i.e. where sequences found in

the analyte solution other than the target sequence also cause displacement of the labeled, pre-hybridized target).

Major parameters that will play a key role are: 1. Length of Sequence; 2. Content of Sequence (GC vs AU vs TA); 3. Uniqueness of sequence (does the genome contain examples of other extremely similar sequences) 4. Analyte solution properties (Ionic strength, pH, etc.); 5. Temperature; 6. Location/Content of mismatched bases (beginning/end of probe vs. middle of probe, AC vs AG vs AA, etc.); 7. Length of Probe (how many/which overlapping bases occur between target and probe strands, does the probe contain overhangs before/after complementary portion); 8. Incubation Time. While 1-3 are a function of the targeted sequence and cannot be varied, 4-8 can be used to tailor probe-target binding.

Another strategy would be to print soluble spots of a labeled target alongside probe spots. This technique would more closely resemble traditional DNA array based assays where fold changes in gene expression are measured by labeling a control group with one label (Cy3 for instance), and an experimental group with a separate label (such as Cy5). However, in this proposed format, only the "control" target is labeled, which is added to the analyte solution as the soluble spots of labeled target dissolve. The degree to which this labeled target binds to the probe spots will be inversely related to the concentration of the unlabeled target sequence present in the analyte solution.

Possible test sequences for initial feasibility:

•miRNA target (mir-155)

5′-UUAAUGCUAAUCGUGAUAGGGGU

•LNA probe

5′-CCTATCACGATTAGCATTAA-biotin

•labeled miRNA targets with partial complementarity (A changed to C, mutation in red)

5′-UUCAUGCUAAUCGUGAUAGGGGU-Cy5

5′-UUCCUGCUAAUCGUGAUAGGGGU-Cy5

5′-UUCCUGCUCAUCGUGAUAGGGGU-Cy5

5′-UUCCUGCUCCUCGUGAUAGGGGU-Cy5

5′-UUCCUGCUCCUCGUGCUAGGGGU-Cy5

5′-UUCCUGCUCCUCGUGCUCGGGGU-Cy5

7.2 Targeted Cell Arrays for Enhanced Immunohistochemistry

Objective: To improve immunohistochemistry through the use of targeted cell arrays based on the following newly developed materials and techniques: 1) An inexpensive, non-fouling surface coating that prevents the non-specific adsorption of cells and proteins,[78] and 2) A simple yet robust method of patterning cell targeting capture agents, such as antibodies, onto this non-fouling surface.[76, 114, 115]

Context: Immunohistochemistry (IHC) plays a crucial role in the field of pathology, and its importance is destined to increase as companion diagnostics are required for new targeted therapeutics. However, the inherent subjectivity of the

assessment of an objective value (the in situ protein concentration) suggests that new technologies are required to achieve the accuracy required for companion diagnostics.[116]

IHC often plays a crucial role in patient care and the determination of course of treatment. An increasing number of drugs are designed to target specific and/or rare cell types, but because of the potential side effects and the high cost of many of these drugs, IHC is often used to predict drug response prior to drug administration.[117] For example, the use of trastuzumab (Herceptin) is only indicated in the treatment of the 20-30% of breast cancers in which the HER2/neu receptor is overexpressed, and prior to the prescription of trastuzumab, breast cancer tumor biopsies must be evaluated by IHC and other methods to determine if HER2 overexpression is in fact present.[118] However, achieving reproducible results by IHC is quite challenging due to a number of sources of variability, which include fixation conditions, specimen pretreatment, reagents, detection methods, washing procedures and interpretation of results.[119, 120] This lack of reproducibility presents a major challenge, and a number of studies have demonstrated the need to improve the quality control measures used in IHC assays.[120-122] In one study of IHC test results for HER2 overexpression, a 15% discordance rate between initial local testing and follow-up central lab testing was found.[123]

Design Principles and Motivation:

1) Individual cells are presented in array format for analysis. The natural morphology of a tissue sample is largely preserved during traditional IHC,[124] and while in some cases this is both necessary and useful, there are many instances where it merely complicates analysis. For instance, if a tissue biopsy is being examined for overexpression of a particular surface receptor, cells do not have to remain embedded in a tissue sample for analysis.[125] By organizing cells into an array, image acquisition and analysis is greatly simplified, whether being conducted by eye or in an automated format.

2) Capture agents specific to the targeted cell type are used to limit the number of extraneous cells. Traditional IHC involves the analysis of whole tissue sections consisting of large numbers of cells, and quite often the majority of these cells are unimportant if the goal is to characterize specific and/or rare cell types. [124] By using surface immobilized capture agents such as antibodies to target specific cell types, it is possible to select for the specific and/or rare cell types of interest. This technique can be used to limit the number of extraneous cells being analyzed, and thereby reduce analysis time, reagent requirements and the potential for false positives as a result.

3) Elimination of Background Noise. Signal-to-noise-ratio and assay interpretation can be significantly improved by eliminating the noise created by non-specific adsorption of labeled detection agents to the substrate background, producing fewer false positives and more sensitive and quantitative results. In addition, wash

procedures can be greatly reduced or even eliminated due to the lack of non-specific adsorption, greatly simplifying assay procedures and improving reliability and reproducibility.

Abbreviated Methods: Surface initiated atom transfer radical polymerization will be used to coat glass slides with poly(oligo(ethylene glycol)methacrylate) (POEGMA). We have recently demonstrated the ability of this non-fouling coating to completely eliminate background noise caused by the non-specific adsorption of cells and proteins in assays conducted in complex biological fluids such as blood and cell lysate.[76] Microspot arrays of anti-HER2/neu antibodies will be printed directly onto the POEGMA surface. These microspots will be created using a remarkably simple method of patterning antibodies onto POEGMA surfaces developed in our lab, which eliminates the need for chemical activation and deactivation to achieve stable antibody microspots on the non-fouling surface and greatly simplifies the fabrication process.[76] In addition, we have shown that antibodies printed onto POEGMA surfaces using this technique have an exceptionally long shelf life under normal ambient conditions, without the need to refrigerate or store in buffer, which makes storage and transport of these arrays much simpler. Breast tumor samples, which have already received a HER2/neu expression score of 0 to 3+, will be used to evaluate the assay. Tumor samples will be treated with collagenase D, and the anti-HER2/neu arrays on POEGMA will be exposed to the resulting cell suspension. HER2/neu positive cells will be captured by the

anti-HER2neu microspots (circular 10um diameter microspots will be used so that there will be approximately 1 cell per microspot), and subsequent labeling with a second anti-Her2/neu antibody will be used to quantify the Her2/neu expression of each cell. Results will be compared to the previously determined HER2/neu expression values of 0 to 3+.

Conclusion: This proposal describes methods that have the potential to make IHC tests more reliable, faster, less expensive and more easily applied at the point of care. HER2/neu expression in breast cancer tumor biopsies represents a potential system for initial proof of principle evaluation.

References

1. Krishnan, S., C.J. Weinman, and C.K. Ober, *Advances in polymers for anti-biofouling surfaces.* Journal of Materials Chemistry, 2008. **18**(29): p. 3405-3413.

2. Gref, R., *The Controlled Intravenous Delivery of Drugs Using PEG-Coated Sterically Stablilized Nanospheres.* Advanced Drug Delivery Reviews, 1995. **16**(2-3): p. 215-233.

3. Hucknall, A., D.H. Kim, S. Rangarajan, R.T. Hill, W.M. Reichert, and A. Chilkoti, *Simple Fabrication of Protein Microarrays on Non-fouling Polymer Brushes With Femtomolar Sensitivity in Serum and Blood.* Advanced Materials, 2009. **21**.

4. Harris, J.M., *Introduction to Biotechnical adn Biomedical Applications of Poly(ethylene glycol)*, in *Poly(Ethylene Glycol) Chemistry: Biotechnical and Biomedical Applications*, J.M. Harris, Editor. 1992, Plenum Press: New York. p. PP. 1-14.

5. Chan, Y.-H.M., *Electrokinetic Characterization of Oligo- and Poly(ethylene glycol)-Terminated Self-Assembled Monolayers on Gold and Glass Surfaces.* Langmuir, 2003. **19**(18): p. 7380-7385.

6. Herrwerth, S., *Factors that Determine the Protein Resistance of Oligoether Self-Assembled Monolayers − Internal Hydrophilicity, Terminal Hydrophilicity, and Lateral Packing Density.* Journal of the American Chemical Society, 2003. **125**(31): p. 9359-9366.

7. Heuberger, M., T. Drobek, and N.D. Spencer, *Interaction Forces and Morphology of a Protein-Resistant Poly(ethylene glycol) Layer.* Biophysical Journal 2005. **88**(1): p. 495-504.

8. Kreuzer, H.J., R.L.C. Wang, and M. Grunze, *Hydroxide Ion Adsorption on Self-Assembled Monolayers.* Journal of the American Chemical Society, 2003. **125**(27): p. 8384-8389.

9. Szleifer, I., *Polymers and proteins: Interactions at interfaces.* Current Opinion in Solid State & Materials Science, 1997. **2**(3): p. 337-344.

10. Andrade, J.D., V. Hlady, and S.I. Jeon. *Poly(ethylene oxide) and protein resistance - Principles, problems, and possibilities*. 1996. Amer Chemical Soc.

11. Jeon, S.I., et al., *Protein Surface Interactions in the Presence of Polyethylene Oxide. 1. Simple Theory.* Journal of Colloid and Interface Science, 1991. **142**(1): p. 149-158.

12. Lee, J.H. and J.D. Andrade, in *Polymer Surface Dynamics*, J.D. Andrade, Editor. 1988, Plenum Press: New York. p. 119-136.

13. Lee, J.H., J. Kopecek, and J.D. Andrade, *Protein-Resistant Surfaces Prepared by Peo-Containing Block Copolymer Surfactants.* Journal of Biomedical Materials Research, 1989. **23**(3): p. 351-368.

14. Elbert, D.L. and J.A. Hubbell, *Reduction of fibrous adhesion formation by a copolymer possessing an affinity for anionic surfaces.* J. Biomed. Mater. Res., 1998. **42**(1): p. 55-65.

15. Liu, V.A., W.E. Jastromb, and S.N. Bhatia, *Engineering protein and cell adhesivity using PEO-terminated triblock polymers.* Journal of Biomedical Materials Research, 2002. **60**(1): p. 126-134.

16. Prime, K.L. and G.M. Whitesides, *Adsorption of Proteins onto Surfaces Containing End-Attached Oligo(Ethylene Oxide) - a Model System Using Self-Assembled Monolayers.* Journal of the American Chemical Society, 1993. **115**(23): p. 10714-10721.

17. Xia, N., et al., *Functionalized poly(ethylene glycol)-grafted polysiloxane monolayers for control of protein binding.* Langmuir, 2002. **18**(8): p. 3255-3262.

18. Bearinger, J.P., et al., *Chemisorbed poly(propylene sulphide)-based copolymers resist biomolecular interactions.* Nature Materials, 2003. **2**(4): p. 259-264.

19. Amiji, M. and K. Park, *Surface Modification of Polymeric Biomaterials with Poly(Ethylene Oxide), Albumin, and Heparin for Reduced Thrombogenicity.* Journal of Biomaterials Science-Polymer Edition, 1993. **4**(3): p. 217-234.

20. Llanos, G.R. and M.V. Sefton, *Does Polyethylene Oxide Possess a Low Thrombogenicity.* Journal of Biomaterials Science-Polymer Edition, 1993. **4**(4): p. 381-400.

21. Lopez, G.P., *Glow-Discharge Plasma Deposition of Tetraethylene Glycol Dimethyl Ether for Fouling-Resistant Biomaterial Surfaces.* Journal of Biomedical Materials Research, 1992. **26**(4): p. 415-439.

22. Hoa, X.D., A.G. Kirk, and M. Tabrizian, *Towards integrated and sensitive surface plasmon resonance biosensors: A review of recent progress.* Biosensors and Bioelectronics, 2007. **23**(2): p. 151-160.

23. Currie, E.P.K., W. Norde, and M.A.C. Stuart, *Tethered polymer chains: surface chemistry and their impact on colloidal and surface properties.* Advances in Colloid and Interface Science, 2003. **100**: p. 205-265.

24. Knoll, D. and J. Hermans, *Polymer-Protein Interactions – Comparison of Experimental and Excluded Volume Theory.* Journal of Biological Chemistry, 1983. **258**(9): p. 5710-5715.

25. Zhu, X.Y., et al., *Grafting of high-density poly(ethylene glycol) monolayers on Si(111).* Langmuir, 2001. **17**(25): p. 7798-7803.

26. Kim, Y.T. and A.J. Bard, *Imaging and Etching of Self Assembled N-octadecanethiol layers on gold with the STM.* Langmuir, 1992. **8**(4): p. 1096-1102.

27. Schonenberger, C., *What are the holes in self assembled monolayers of alkanethiols on gold.* Langmuir, 1994. **10**(3): p. 611-614.

28. Zhao, X.M., J.L. Wilbur, and G.M. Whitesides, *Using two-stage chemical amplification to determine the density of defects in self-assembled monolayers of alkanethiolates on gold.* Langmuir, 1996. **12**(13): p. 3257-3264.

29. Schoenfisch, M.H. and J.E. Pemberton, *Air stability of alkanethiol self-assembled monolayers on silver and gold surfaces.* Journal of the American Chemical Society, 1998. **120**(18): p. 4502-4513.

30. Tarlov, M.J. and J.G. Newman, *Static secondary ion mass spectrometry of self assembled alkanethiol monolyers on gold.* Langmuir, 1992. **8**(5): p. 1398-1405.

31. Ma, H.W., *"Non-fouling" oligo(ethylene glycol)-functionalized polymer brushes synthesized by surface-initiated atom transfer radical polymerization.* Advanced Materials, 2004. **16**(4): p. 338.

32. Hyun, J. and A. Chilkoti, *Surface-initiated free radical polymerization of polystyrene micropatterns on a self-assembled monolayer on gold.* Macromolecules, 2001. **34**(16): p. 5644-5652.

33. Prucker, O. and J. Ruhe, *Polymer layers through self-assembled monolayers of initiators.* Langmuir, 1998. **14**(24): p. 6893-6898.

34. Huang, N.P., et al., *Poly(L-lysine)-g-poly(ethylene glycol) layers on metal oxide surfaces: Surface-analytical characterization and resistance to serum and fibrinogen adsorption.* Langmuir, 2001. **17**(2): p. 489-498.

35. Jordan, R., et al., *Surface-initiated anionic polymerization of styrene by means of self-assembled monolayers.* Journal of the American Chemical Society, 1999. **121**(5): p. 1016-1022.

36. Jordan, R. and A. Ulman, *Surface initiated living cationic polymerization of 2-oxazolines.* Journal of the American Chemical Society, 1998. **120**(2): p. 243-247.

37. Weck, M., et al., *Ring-opening metathesis polymerization from surfaces.* Journal of the American Chemical Society, 1999. **121**(16): p. 4088-4089.

38. Jeon, N.L., et al., *Patterned polymer growth on silicon surfaces using microcontact printing and surface-initiated polymerization.* Applied Physics Letters, 1999. **75**(26): p. 4201-4203.

39. Kratzmuller, T., D. Appelhans, and H.G. Braun, *Ultrathin microstructured polypeptide layers by surface- initiated polymerization on microprinted surfaces.* Advanced Materials, 1999. **11**(7): p. 555-+.

40. Choi, I.S. and R. Langer, *Surface-initiated polymerization of L-lactide: coating of solid substrates with a biodegradable polymer.* Macromolecules, 2001. **34**(16): p. 5361-5363.

41. Velten, U., et al., *Polymerization of styrene with peroxide initiator ionically bound to high surface area mica.* Macromolecules, 1999. **32**(11): p. 3590-3597.

42. Severini, F., et al., *Free radical grafting of maleic anhydride in vapour phase on polypropylene film.* Polymer, 1999. **40**(25): p. 7059-7064.

43. Fujiki, K., et al., *Radical grafting from glass fiber surface: Graft polymerization of vinyl monomers initiated by azo groups introduced onto the surface.* Journal of Polymer Science Part a-Polymer Chemistry, 1999. **37**(13): p. 2121-2128.

44. Husseman, M., et al., *Controlled synthesis of polymer brushes by "living" free radical polymerization techniques.* Macromolecules, 1999. **32**(5): p. 1424-1431.

45. Huang, X. and M.J. Wirth, *Surface initiation of living radical polymerization for growth of tethered chains of low polydispersity.* Macromolecules, 1999. **32**(5): p. 1694-1696.

46. Matyjaszewski, K., et al., *Polymers at interfaces: using atom transfer radical polymerization in the controlled growth of homopolymers and block copolymers from silicon surfaces in the absence of untethered sacrificial initiator.* Macromolecules, 1999. **32**(26): p. 8716-8724.

47. Zhao, B. and W.J. Brittain, *Polymer brushes: surface-immobilized macromolecules.* Progress in Polymer Science, 2000. **25**(5): p. 677-710.

48. Ma, H.W., et al., *Protein-resistant polymer coatings on silicon oxide by surface-initiated atom transfer radical polymerization.* Langmuir, 2006. **22**(8): p. 3751-3756.

49. Ma, H.W., et al., *Surface-initiated atom transfer radical polymerization of oligo(ethylene glycol) methyl methacrylate from a mixed self-assembled monolayer on gold.* Advanced Functional Materials, 2006. **16**(5): p. 640-648.

50. Brown, A.A., et al., *Synthesis of oligo(ethylene glycol) methacrylate polymer brushes.* European Polymer Journal, 2005. **41**(8): p. 1757-1765.

51. Prucker, O.R., J., *Mechanism of Radical Chain Polymerizations Initiated by Azo Compounds Covalently Bound to the Surface of Spherical Particles* Macromolecules, 1998. **31**(3): p. 602-613.

52. Ejaz, M.Y., S.; Ohno, K.; Tsujii, Y.; Fukuda, T., *Controlled Graft Polymerization of Methyl Methacrylate on Silicon Substrate by the Combined Use of the Langmuir-Blodgett and Atom Transfer Radical Polymerization Techniques* Macromolecules, 1998. **31**(17): p. 5934-5936.

53. Tugulu, S., et al., *RGD - Functionalized polymer brushes as substrates for the integrin specific adhesion of human umbilical vein endothelial cells.* Biomaterials, 2007. **28**(16): p. 2536-2546.

54. Fan, X.W., et al., *Biomimetic anchor for surface-initiated polymerization from metal substrates.* Journal of the American Chemical Society, 2005. **127**(45): p. 15843-15847.

55. Katira, P., et al., *Quantifying the performance of protein-resisting surfaces at ultra-low protein coverages using kinesin motor proteins as probes.* Advanced Materials, 2007. **19**(20): p. 3171-+.

56. Holmlin, R.E., et al., *Zwitterionic SAMs that Resist Nonspecific Adsorption of Protein from Aqueous Buffer.* Langmuir, 2001. **17**(9): p. 2841-2850.

57. Ladd, J., et al., *Zwitterionic Polymers Exhibiting High Resistance to Nonspecific Protein Adsorption from Human Serum and Plasma.* Biomacromolecules, 2008. **9**(5): p. 1357-1361.

58. Lee, B.S., et al., *Functionalization of Poly(oligo(ethylene glycol) methacrylate) Films on Gold and Si/SiO2 for Immobilization of Proteins and Cells: SPR and QCM Studies.* Biomacromolecules, 2007. **8**(12): p. 3922-3929.

59. Xu, F.J., et al., *Spatially well-defined binary brushes of poly(ethylene glycol)s for micropatterning of active proteins on anti-fouling surfaces.* Biosensors & Bioelectronics, 2008. **24**(4): p. 773-780.

60. Lutz, J.F., H.G. Borner, and K. Weichenhan, *Combining ATRP and "click" chemistry: a promising platform toward functional biocompatible polymers and polymer bioconjugates (vol 39, pg 6376, 2006).* Macromolecules, 2007. **40**(19): p. 7060-7060.

61. Angenendt, P., *Progress in protein and antibody microarray technology.* Drug Discovery Today, 2005. **10**(7): p. 503-511.

62. Haab, B.B., *Methods and applications of antibody microarrays in cancer research.* Proteomics, 2003. **3**(11): p. 2116-2122.

63. Kingsmore, S.F., *Multiplexed protein measurement: technologies and applications of protein and antibody arrays.* Nature Reviews Drug Discovery, 2006. **5**(4): p. 310-320.

64. Kusnezow, W. and J.D. Hoheisel, *Solid supports for microarray immunoassays.* Journal of Molecular Recognition, 2003. **16**(4): p. 165-176.

65. MacBeath, G., *Protein microarrays and proteomics.* Nature Genetics, 2002. **32**: p. 526-532.

66. Wingren, C. and C.A.K. Borrebaeck, *Antibody microarrays: Current status and key technological advances.* Omics-a Journal of Integrative Biology, 2006. **10**(3): p. 411-427.

67. Coleman, M.A., et al., *Applications of functional protein microarrays - Identifying protein-protein interactions in an array format*, in *Methods in Molecular Biology*, P.N. Floriano, Editor. 2007, Humana Press Inc. p. 121-130.

68. Zhu, H., et al., *Analysis of yeast protein kinases using protein chips.* Nature Genetics, 2000. **26**(3): p. 283-289.

69. Popescu, S.C., et al., *Differential binding of calmodulin-related proteins to their targets revealed through high-density Arabidopsis protein microarrays.* Proceedings of the National Academy of Sciences of the United States of America, 2007. **104**(11): p. 4730-4735.

70. Gao, W.M., et al., *Distinctive serum protein profiles involving abundant proteins in lung cancer patients based upon antibody microarray analysis.* Bmc Cancer, 2005. **5**: p. 10.

71. Spisak, S., et al., *Protein microchips in biomedicine and biomarker discovery.* Electrophoresis, 2007. **28**(23): p. 4261-4273.

72. Wood, W.G. *Matrix effects in immunoassays*. 1991. Scandinavian University Press.

73. Selby, C., *Interference in immunoassay.* Annals of Clinical Biochemistry, 1999. **36**: p. 704-721.

74. Low, N.M., P. Holliger, and G. Winter, *Mimicking Somatic Hypermutation: Affinity Maturation of Antibodies Displayed on Bacteriophage Using a Bacterial Mutator Strain.* Journal of Molecular Biology, 1996. **260**(3): p. 359-368.

75. Leng, S.X., et al., *ELISA and Multiplex Technologies for Cytokine Measurement in Inflammation and Aging Research.* J Gerontol A Biol Sci Med Sci, 2008. **63**(8): p. 879-884.

76. Hucknall, A., et al., *Simple Fabrication of Antibody Microarrays on Nonfouling Polymer Brushes with Femtomolar Sensitivity for Protein Analytes in Serum and Blood.* Advanced Materials, 2009. **21**(19): p. 1968-1971.

77. Hucknall, A., et al., *Versatile synthesis and micropatterning of nonfouling polymer brushes on the wafer scale.* Biointerphases, 2009. **4**: p. FA50-FA57.

78. Hucknall, A., S. Rangarajan, and A. Chilkoti, *In Pursuit of Zero: Polymer Brushes that Resist the Adsorption of Proteins.* Adv. Mater., 2009. **21**: p. 2441-2446.

79. Derby, B., *Bioprinting: inkjet printing proteins and hybrid cell-containing materials and structures.* Journal of Materials Chemistry, 2008. **18**(47): p. 5717-5721.

80. Branson, B.M., *Point-of-Care Rapid Tests for HIV Antibody.* Jounal of Laboratory Medicine, 2003. **27**(7/8): p. 288-295.

81. Taylor, G.N. and T.M. Wolf, *Oxygen Plasma Removal of think polymer films.* Polymer Engineering and Science, 1980. **20**(16): p. 1087-1092.

82. Briggs, D., ed. *Surface analysis of polymers by XPS and static SIMS*. Cambridge Solid State Science Series. 1998, Cambridge University Press: New York.

83. Ma, H., et al., *Protein resistant polymer brushes on silicon oxide by surface initiated atom transfer radical polymerization.* Langmuir, 2006. **22**: p. 3751 -3756.

84. Zhang, Z., et al., *Pretreatment of Amphiphilic Comb Polymer Surfaces Dramatically Affects Protein Adsorption.* Biomacromolecules, 2005. **6**(6): p. 3388-3396.

85. Massia, S.P. and J.A. Hubbell, *An RGD spacing of 440NM is sufficient for Integrin Alpha-V-Beta-3 mediated fibroblast spreading and 140NM for focal contact and stress fiber formation.* Journal of Cell Biology, 1991. **114**(5): p. 1089-1100.

86. Harbers, G.M. and K.E. Healy, *The effect of ligand type and density on osteoblast adhesion, proliferation, and matrix mineralization.* Journal of Biomedical Materials Research Part A, 2005. **75A**(4): p. 855-869.

87. Wood, W.G., *Matrix Effects in Immunoassays.* Scandinavian Journal of Clinical and Laboratory Investigation, 1991. **51**(1 supp 205): p. 105 - 112.

88. Dressick, W.J., et al., *Proximity x-ray lithography of siloxane and polymer films containing benzyl chloride functional groups.* J. Vac. Sci. Technol. A, 1999. **17**(4): p. 1432-1440.

89. Buckley, C.E. and F.C. Dorsey, *Serum Immunoglobulin Levels Throughout the Life-Span of Healthy Man.* Annals of Internal Medicine, 1971. **75**(5): p. 673-682.

90. *British Heart Foundation Heath Promotion Research Group.* Department of Public Health University of Oxford.

91. *Health Economics Research Centre, Department of Public Health, Univeristy of Oxford*

92. *AHA Heart Disease and Stroke Statistics 2008 Access date: 3/20/2009* <http://www.americanheart.org/presenter.jhtml?identifier=3000090>.

93. Apple, F.S., et al., *Role of Monitoring Changes in Sensitive Cardiac Troponin I Assay Results for Early Diagnosis of Myocardial Infarction and Prediction of Risk of Adverse Events.* Clinical Chemistry, 2009. **55**(5): p. 930-937.

94. Krupicka, J., et al., *Natriuretic Peptides - Physiology, Pathophysiology and Clinical Use in Heart Failure.* Physiological Research, 2009. **58**(2): p. 171-177.

95. Michel, R., et al., *Influence of PEG Architecture on Protein Adsorption and Conformation.* Langmuir, 2005. **21**(26): p. 12327-12332.

96. *Department of Health and Human Services, Agency for Healthcare Research and Quality, National estimates on hospital use for all patients from the HCUP Nationwide Inpatient Sample, Number of Open Prostate Procedures, 2009. http://hcupnet.ahrq.gov/HCUPnet.jsp accessed on 11/15/2011.*

97. Hong, S.K., et al., *Prognostic Significance of Undetectable Ultrasensitive Prostate-specific Antigen Nadir After Radical Prostatectomy.* Urology, 2010. **76**(3): p. 723-727.

98. Doherty, A.P., et al., *Undetectable ultrasensitive PSA after radical prostatectomy for prostate cancer predicts relapse-free survival.* British Journal of Cancer, 2000. **83**(11): p. 1432-1436.

99. Eisenberg, M.L., et al., *Prognostic Implications of an Undetectable Ultrasensitive Prostate-Specific Antigen Level after Radical Prostatectomy.* European Urology, 2010. **57**(4): p. 622-630.

100. Sakai, I., et al., *Usefulness of the Nadir Value of Serum Prostate-Specific Antigen Measured by an Ultrasensitive Assay as a Predictor of Biochemical Recurrence after Radical Prostatectomy for Clinically Localized Prostate Cancer.* Urologia Internationalis, 2006. **76**(3): p. 227-231.

101. Shen, S., et al., *Ultrasensitive serum prostate specific antigen nadir accurately predicts the risk of early relapse after radical prostatectomy.* Journal of Urology, 2005. **173**(3): p. 777-780.

102. Moreira, D.M., et al., *Postoperative prostate-specific antigen nadir improves accuracy for predicting biochemical recurrence after radical prostatectomy: Results from the Shared Equal Access Regional Cancer Hospital (SEARCH) and Duke Prostate Center databases.* International Journal of Urology, 2010. **17**(11): p. 914-922.

103. Bock, J.L. and G.G. Klee, *How sensitive is a prostate-specific antigen measurement? How sensitive does it need to be?* Archives of pathology & laboratory medicine, 2004. **128**(3): p. 341-343.

104. Thompson, I.M., et al., *Adjuvant Radiotherapy for Pathological T3N0M0 Prostate Cancer Significantly Reduces Risk of Metastases and Improves Survival: Long-Term Followup of a Randomized Clinical Trial.* The Journal of Urology, 2009. **181**(3): p. 956-962.

105. Trock, B.J., et al., *Prostate Cancer–Specific Survival Following Salvage Radiotherapy vs Observation in Men With Biochemical Recurrence After Radical Prostatectomy.* JAMA: The Journal of the American Medical Association, 2008. **299**(23): p. 2760-2769.

106. Stephenson, A.J., et al., *Salvage Radiotherapy for Recurrent Prostate Cancer After Radical Prostatectomy.* JAMA: The Journal of the American Medical Association, 2004. **291**(11): p. 1325-1332.

107. Stephenson, A.J., et al., *Predicting the Outcome of Salvage Radiation Therapy for Recurrent Prostate Cancer After Radical Prostatectomy.* Journal of Clinical Oncology, 2007. **25**(15): p. 2035-2041.

108. Gorton, L., ed. *Biosensors and modern biospecific analytical techniques* 2005, Elsevier: Boston.

109. Ehrenkranz, J.R.L., *Home and Point-of-Care Pregnancy Tests: A Review of the Technology.* Epidemiology, 2002. **13**(3): p. S15-S18.

110. Goluch, E.D., et al., *A bio-barcode assay for on-chip attomolar-sensitivity protein detection.* Lab on a Chip, 2006. **6**(10): p. 1293-1299.

111. Lauhon, L.J., et al., *Epitaxial core-shell and core-multishell nanowire heterostructures.* Nature, 2002. **420**(6911): p. 57-61.

112. Sano, T., C.L. Smith, and C.R. Cantor, *IMMUNO-PCR - VERY SENSITIVE ANTIGEN-DETECTION BY MEANS OF SPECIFIC ANTIBODY-DNA CONJUGATES.* Science, 1992. **258**(5079): p. 120-122.

113. Taton, T.A., C.A. Mirkin, and R.L. Letsinger, *Scanometric DNA array detection with nanoparticle probes.* Science, 2000. **289**(5485): p. 1757-1760.

114. Ainsworth, R., et al., *IHC for Her2 with CBE356 antibody is a more accurate predictor of Her2 gene amplification by FISH than HercepTest™ in breast carcinoma.* Journal of Clinical Pathology, 2005. **58**(10): p. 1086-1090.

115. Tan, C.P., et al., *Parylene peel-off arrays to probe the role of cella[euro sign]"cell interactions in tumour angiogenesis.* Integrative Biology, 2009. **1**(10): p. 587-594.

116. Cregger, M., A. Berger, and D. Rimm, *Immunohistochemistry and quantitative analysis of protein expression.* Archives of pathology & laboratory medicine, 2006. **130**(7): p. 1026-1030.

117. Papadopoulos, N., K. Kinzler, and B. Vogelstein, *The role of companion diagnostics in the development and use of mutation-targeted cancer therapies.* Nature biotechnology, 2006. **24**(8): p. 985-995.

118. Bange, J., E. Zwick, and A. Ullrich, *Molecular targets for breast cancer therapy and prevention.* Nature Medicine, 2001. **7**(5): p. 548.

119. O'Leary, T., *Standardization in immunohistochemistry.* Applied Immunohistochemistry & Molecular Morphology, 2001. **9**(1): p. 3.

120. Paik, S., et al., *Real-world performance of HER2 testing—national surgical adjuvant breast and bowel project experience.* Journal of the National Cancer Institute, 2002. **94**(11): p. 852.

121. Perez, E., et al., *HER2 testing by local, central, and reference laboratories in specimens from the North Central Cancer Treatment Group N9831 intergroup adjuvant trial.* Journal of Clinical Oncology, 2006. **24**(19): p. 3032.

122. O'Malley, F., et al., *HER2 testing in a population-based study of patients with metastatic breast cancer treated with trastuzumab.* Archives of pathology & laboratory medicine, 2008. **132**(1): p. 61.

123. Roche, P., et al., *Concordance between local and central laboratory HER2 testing in the breast intergroup trial N9831.* Journal of the National Cancer Institute, 2002. **94**(11): p. 855.

124. Ramos-Vara, J., *Technical aspects of immunohistochemistry.* Veterinary Pathology Online, 2005. **42**(4): p. 405.

125. Al-Hajj, M., et al., *Prospective identification of tumorigenic breast cancer cells.* Proceedings of the National Academy of Sciences of the United States of America, 2003. **100**(7): p. 3983..

Biography

Angus Hucknall attended North Carolina State University, where he received bachelor's degrees in Textile Chemistry, Spanish and Chemistry. He also attended the Massachusettes Institue of Technology, where he received a master's degree in Materials Science. His current list of publications is as follows:

1)A Hucknall, A Garcia, MS Johannes, AJ Simnick, RT Hill, BD Ratner, RL Clark, S Zauscher, and A Chilkoti, Substrate-independent synthesis and micro-patterning of non-fouling polymer brushes on the wafer-scale, Biointerphases 4: FA 50-FA57 (2009).
2)A Hucknall, S Rangarajan, and A Chilkoti, In pursuit of zero: Polymer brushes that resist the adsorption of proteins, Adv. Mater., 21: 2441-2446 (2009).
3)A Hucknall, D Kim, S Rangarajan, W Reichert, and A Chilkoti, Simple fabrication of antibody microarrays on non-fouling polymer brushes with femtomolar sensitivity for protein analytes in serum and blood, Adv. Mater. 21:1968-1971 (2009).
4)RT Hill, KM Kozek, A Hucknall, DR Smith, A Chilkoti. Nanoparticle-Film Plasmon Ruler Interrogated with Transmission Visible Spectroscopy.ACS Photonics 1.10 (2014)
5)V Tjong, H Yu, A Hucknall and A Chilkoti.Direct Fluorescence Detection of RNA on Microarrays by Surface-Initiated Enzymatic Polymerization. Analytical Chemistry.(2013)
6)RT Hill, JJ Mock, A Hucknall, SD Wolter, NM Jokerst, DR Smith and A Chilkoti.Plasmon Ruler with Angstrom Length Resolution. ACS Nano 6.10 (2012)
7)R Ferris, A Hucknall, BS Kwon, T Chen, A Chilkoti and S Zauscher, Field-induced nanolithography for patterning of non-fouling polymer brush surfaces, Small, 7: (2011).
8)V Tjong, H Yu, A Hucknall, S Rangarajan and A Chilkoti, Amplified On-Chip Fluorescence Detection of DNA Hybridization by Surface-Initiated Enzymatic Polymerization, Analytical Chemistry, 83: 5153-5159 (2011).
9)S Alang-Ahmad, A Hucknall, A Chilkoti, and GJ Leggett, Micro- and nano-structured poly(oligo(ethylene glycol)methacrylate) brushes grown from photopatterned halogen initiators by atom transfer radical polymerization, Biointerphases, 6: 8-15 (2011)
10)S Alang-Ahmad, A Hucknall, A Chilkoti, and GJ Leggett, Protein patterning by UV-induced photodegradation of poly(oligo(ethylene glycol)methacrylate) brushes, Langmuir, 26: 9937–9942 (2010).
11)NJ Jenness, RT Hill, A Hucknall, A Chilkoti and RL Clark, A versatile diffractive maskless lithography for single-shot and serial microfabrication, Optics Express, 18: 11754-11762 (2010).
12)F Gelain, X Wang, A Horii, A Hucknall, S Koutsopoulos and S Zhang, Designer Self-Assembling Peptide Scaffolds for 3D Tissue Cell Cultures, Methods in Bioengineering: 3D Tissue Engineering, 59-81 (2010).